# AN INTEGRATIVE APPROACH FOR ENVIRONMENTAL ASSESSMENT AND WATER RESOURCES MANAGEMENT USING DIRECT CURRENT RESISTIVITY (DC), GEOGRAPHIC INFORMATION SYSTEM (GIS), REMOTE SENSING, AND GAIN AND LOSS METHOD

by

Dina Ragab Desouki Abdelmoneim

A thesis

submitted in partial fulfillment

of the requirements for the degree of

Master of Science in (Hydrologic Sciences)

Boise State University

August 2021

BOISE STATE UNIVERSITY GRADUATE COLLEGE

# DEFENSE COMMITTEE AND FINAL READING APPROVALS

of the thesis submitted by

Dina Ragab Desouki Abdelmoneim

Thesis Title: An Integrative Approach for Environmental Assessment and Water Resources Management Using Direct Current Resistivity (DC), Geographic Information System (GIS), Remote Sensing, and Gain and Loss Method

Date of Final Oral Examination: 1 July 2021

The following individuals read and discussed the thesis submitted by student Dina Ragab Desouki Abdelmoneim, and they evaluated their presentation and response to questions during the final oral examination. They found that the student passed the final oral examination.

| | |
|---|---|
| Alejandro Flores, Ph.D. | Chair, Supervisory Committee |
| Kendra Kaiser, Ph.D. | Member, Supervisory Committee |
| Qifei Nui, Ph.D. | Member, Supervisory Committee |

The final reading approval of the thesis was granted by Alejandro Flores, Ph.D., Chair of the Supervisory Committee. The thesis was approved by the Graduate College.

# DEDICATION

This work is dedicated to,

People who did and did not believe in me,

My fantastic family; parents, brother, sister, and my husband,

And to my lovely son, Malik without whom, I would have finished this thesis earlier.

ACKNOWLEDGMENTS

The completion of this work would not have been possible without the generous support by a large number of people who are too many to name here. My supervisory committee members, Dr. Alejandro Flores, Dr. Kendra Kaiser, and Dr. Qifei Nui deserve a heartfelt thank you for their guidance, instructions, advising, and support during the last couple of years of my life. Indeed, the friendship that has formed over the last couple of years is among my most treasured. I want to thank the LEAF group, Dr. McNamara, and all the members of the Geosciences department at Boise State University for always being supportive and generous with their time. As well, I would like to acknowledge and thank Fulbright for funding me throughout this project. Thank you to the Pioneer district, IDWR, USGS, City of Nampa, Lions Park staff, Geophysics lab, Dr. Attwa, and the National Research Centre in Egypt for their help and support. Additionally, I would like to thank my wonderful family, especially my mom, dad, brother, sister, husband, and my best supporter; sweet son Malik for always supporting and encouraging me to follow my passion and my dreams. Finally, and most importantly, I would like to thank ALLAH without whom I would have been lost.

# ABSTRACT

Sustainable water resource management is a crucial national and global issue (Currell et al., 2012). In arid areas, groundwater is often the major source of water or at least a crucial supplement to other freshwater resources for agriculture, industry and domestic consumption (Vrba and Renaud, 2016). The complexity associated with groundwater-surface water interactions creates uncertainty about water resource sustainability in semi-arid environments, especially with urbanization and population growth. Flood irrigation in the early 1900s increased the shallow groundwater table in the Treasure Valley (TV), but with increasing irrigation efficiencies, they have been declining since the 1960s with a mean decline rate of about 2.9-3.9x10^-9 (m/s) (Contor et al., 2011). Quantifying how much surface water is being exchanged with the shallow groundwater table through canals in the TV is necessary for gaining a better understanding of groundwater-surface water interactions in this heavily managed system. This knowledge would help evaluate alternative management options for achieving sustainable management of existing water resources.

The key objectives of this project are to determine the seepage rate through some canal reaches in the TV, evaluate the integration of the gain and loss method, remote sensing, GIS, hydrogeophysical simulation, and direct current (DC) resistivity geophysical methods for water resource management. We hypothesize that the underlying lithology and size of canals affect the magnitude of the seepage rate. Flow measurements were collected

weekly between July and August 2020 in canal reaches representing different sizes and lithological units to determine the seepage rate using the reach gain/loss method. Canal variability and measurement uncertainty were included in seepage estimation for the entire TV using 3 alternative scaling approaches. DC resistivity was used as a complementary method to monitor the seepage effect on the shallow GW aquifer over 2 months. This research evaluates to what extent canal size and its underlying lithology affects the seepage rate, and how the integration of methods may provide additional insight into groundwater exchange-surface water.

TABLE OF CONTENTS

LIST OF TABLES

LIST OF FIGURES

LIST OF PHOTOS

## LIST OF ABBREVIATIONS

| | |
|---|---|
| Af | Acre feet |
| Acre.ft/yr | Acre feet per year |
| Cfs | cubic feet per second |
| Cms | cubic meter per second |
| DEM | Digital Elevation Model |
| ESRP | Eastern Snake River Plain |
| ET | Evapotranspiration |
| ERT | Electrical Resistivity Tomography |
| ERI | Electrical Resistivity Imaging |
| G/L | Gain/Loss |
| GW | Groundwater |
| IDWR | Idaho Department of Water Resources |
| MAR | Managed aquifer recharge |
| SW | Surface Water |
| TV | Treasure Valley |
| TVHP | Treasure Valley Hydrologic project |
| USGS | United States Geological Survey |
| WY | Water Year |
| WSRP | Western Snake River Plain |
| 3D HFM | Three-dimensional hydrogeologic framework model |

# CHAPTER 1: INTRODUCTION AND OVERVIEW

Sustainable water resource management is a crucial national and global issue (Currell et al., 2012). Traditionally, it has focused on surface water or groundwater as separate entities, but with land and water resources development, it is apparent that changes in quantity and quality of either one of them affect the other because both groundwater and surface water are in many cases connected (Winter et al., 1998). In arid areas, groundwater is often a major source of water, or at least a crucial supplement to other freshwater resources, for agriculture, industry and domestic consumptions (Vrba and Renaud, 2016). Thus, groundwater in arid areas needs to be robustly understood to avoid diminishing groundwater supplies and to ensure a sustainable use of groundwater resources (Famiglietti, 2014; Dalin et al., 2017; Rodell et al., 2018). Population growth and land use change in the form of urbanization create additional uncertainty about water resource sustainability in semi-arid environments. As a result of the uncertainty of a sustainable groundwater future, concern for future water resources has spurred research into evaluating the status of current water resources in order to create strategies to meet future needs (Williams, 2011). The recharge–discharge balance has been fundamentally altered and pumping has created a massive deficit between extraction and replenishment (Currell et al., 2012).

Long term directional change in groundwater levels can have a range of consequences for local to regional planning and development priorities. An excessive increase in groundwater levels may damage infrastructure, urban development, or affect

agriculture due to high salinity caused by high evaporation rates. Changing water and salt balances can cause soil salinity, desertification and ecosystem degradation (Cui and Shao, 2005). This has been mitigated in some areas by improved irrigation technology such as drip irrigation, and advancements in sprinkler systems, increased regulation and oversight, or a combination of strategies.

Globally, groundwater levels have declined where withdrawal rates are greater than recharge rates (Kemper, 2004). This has led to various environmental impacts such as ground subsidence (Contor et al., 2011) as well as drying of wetlands and streams – even when the total groundwater storage in a basin remains high (Llamas & Custodio, 2002). An excessive decrease in groundwater levels in the future could cause several environmental hazards such as slope failure, subsidence, and even landslides induced by perched aquifers (Contor et al., 2011). Moreover, groundwater temperatures may rise by the upwelling of deeper thermal waters via fault conduits which would limit the potential development of the deeper cold water aquifer and require cautious plans for any further drilling settings (Contor et al., 2011).

Storing water exceeding the current needs in the aquifer for future withdrawal when capacities are low, known as managed aquifer recharge (MAR), may be a valuable mechanism for avoiding water shortage and potential hazards. Globally, MAR is increasingly being used to increase groundwater storage. There are various mechanisms for increasing aquifer recharge, such as creating artificial surface streams and ponds (“spreading grounds") in fast-draining soil which require delivery structures such as canals to deliver surface water to these locations.

The key elements replenishing the groundwater aquifers in intensively managed systems such as the Treasure Valley (TV) are direct infiltration from agricultural irrigation and seepage from canals. It is essential to precisely measure how much water is being used in this intensively managed system for better managing its existing water resources, but the measurement accuracy of water flow and volume through the irrigation system is affected by many factors such as Evapotranspiration (ET), runoff from fields and yards, water flow measurement variability, and canal seepage. The latter is the largest component of groundwater aquifer recharge in TV. Newton (1991) stated that 80% of the total recharge to the WSRP aquifer system was from infiltration of surface-water irrigation including canal seepage, while Urban (2004) estimated that 62% and 50% of the total groundwater aquifer recharge in the TV for the 1996 and 2000 irrigation years, respectively, are attributable to the irrigation canal seepage. However, the combined Schmidt et al. (2008) and Sukow (2012) budgets estimated that 48% and 46% of the total recharge are attributed to the canal seepage and on-farm infiltration, respectively. The estimation of the canal seepage in these budgets is based on the total length of the major canals which extends to approximately 1,882,932 m (IDWR, 1997) in the canal system of the TV and seepage estimates of smaller supplies and ditches are not provided (Urban, 2004). We hypothesize that both canal properties (i.e. size and lithology), and measurement variability control the estimation of incidental seepage magnitude through the canal system. The objective of this thesis is to quantify the magnitude of recharge through canals and characterize the factors that affect its spatial variability. Quantifying how much surface water is being exchanged with the shallow groundwater table through canals (including the smaller drains and supplies) is necessary for gaining a better understanding of groundwater-surface water

interactions in the heavily managed systems. This knowledge would help evaluate alternative management options for achieving sustainable management of the existing water resources. This objective will be accomplished using the reach gain and loss method, and Electrical Resistivity Tomography (ERT).

### 1.1 Groundwater - Surface Water Interaction

Groundwater (GW) interactions with surface water (SW) are common features of almost all hydrologic systems and natural surface water bodies like rivers, wetlands, and lakes are often manifestations of these interactions (Khan et al., 2019). GW-SW interactions can be of three types; losing water to the underlying aquifer, gaining water from the underlying aquifer, or gaining water from the aquifers in some locations and losing in others (Jolly et al., 2008). GW-SW interactions are usually controlled by head differences between SW and GW, local geomorphology, especially the texture and chemistry of soils, and the GW flow geometry (Kumar, 2018). Some locations may shift in time from losing to gaining in response to climate, land use, and management that affect SW levels and the underlying GW levels over time (Kumar, 2018). In addition to the quantities of water exchanged between GW and SW, water quality is also of importance as groundwater contaminants can ultimately "daylight" in surface water systems and vice versa (Winter et al., 1998). GW-SW interactions are difficult to observe and measure and their complexity creates uncertainty about water resource sustainability in semi-arid environments, especially with urbanization and population growth. These interactions are significantly variable in time and space, however a basic understanding of the relationships between these two systems is essential for better management and appropriate strategic planning on water-resource issues.

## 1.2 Study Area: Treasure Valley

The Snake River Plain, located in southwestern Idaho in the western United States is approximately 48,280 m wide in the section containing the lower Boise River. The lower Boise River system begins when the Boise River exits the mountains near Lucky Peak Reservoir and extends almost 102,998 m northwestward through the TV until its confluence with the Snake River. The western Snake River Plain (WSRP), the northwest-trending topographic depression formed by crustal extension, beginning as early as 17 million years ago (Malde, 1991), is a relatively flat lowland separating the Cretaceous-age granitic mountains of west-central Idaho from the granitic/volcanic Owyhee mountains in southwestern Idaho and extends from about Twin Falls, Idaho northwestward to Vale, Oregon. The region known locally as the Treasure Valley (TV, Figure 1.1) is located within the WSRP, and encompasses the lower Boise River, as well as lowland portions of the Payette, Weiser, Malheur, Owyhee, and Burnt rivers. It is the agricultural area that stretches west from Boise to Oregon (U.S. Board on Geographic Names, 2019). The valley is surrounded to the north by the Boise Foothills and is relatively flat with some rolling hills within the southernmost portion of the area. It is the most populated area in Idaho and it includes all the lowland areas from Vale in rural eastern Oregon to Boise. The TV includes a portion of Oregon, but we are focusing on Idaho in this study. The study area includes most of both Ada and Canyon counties with a total area of about 4.7x10^9 sq. meter where 2891 canal reaches of 5,813,852 m total length are crossing it (Figure 1.2). The TV's irrigation canal system is regulated by irrigation districts which are typically formed to develop new irrigation projects or acquire existing irrigation projects. Irrigation districts possess water rights, as well as diversion facilities and infrastructure (Figure 1.3).

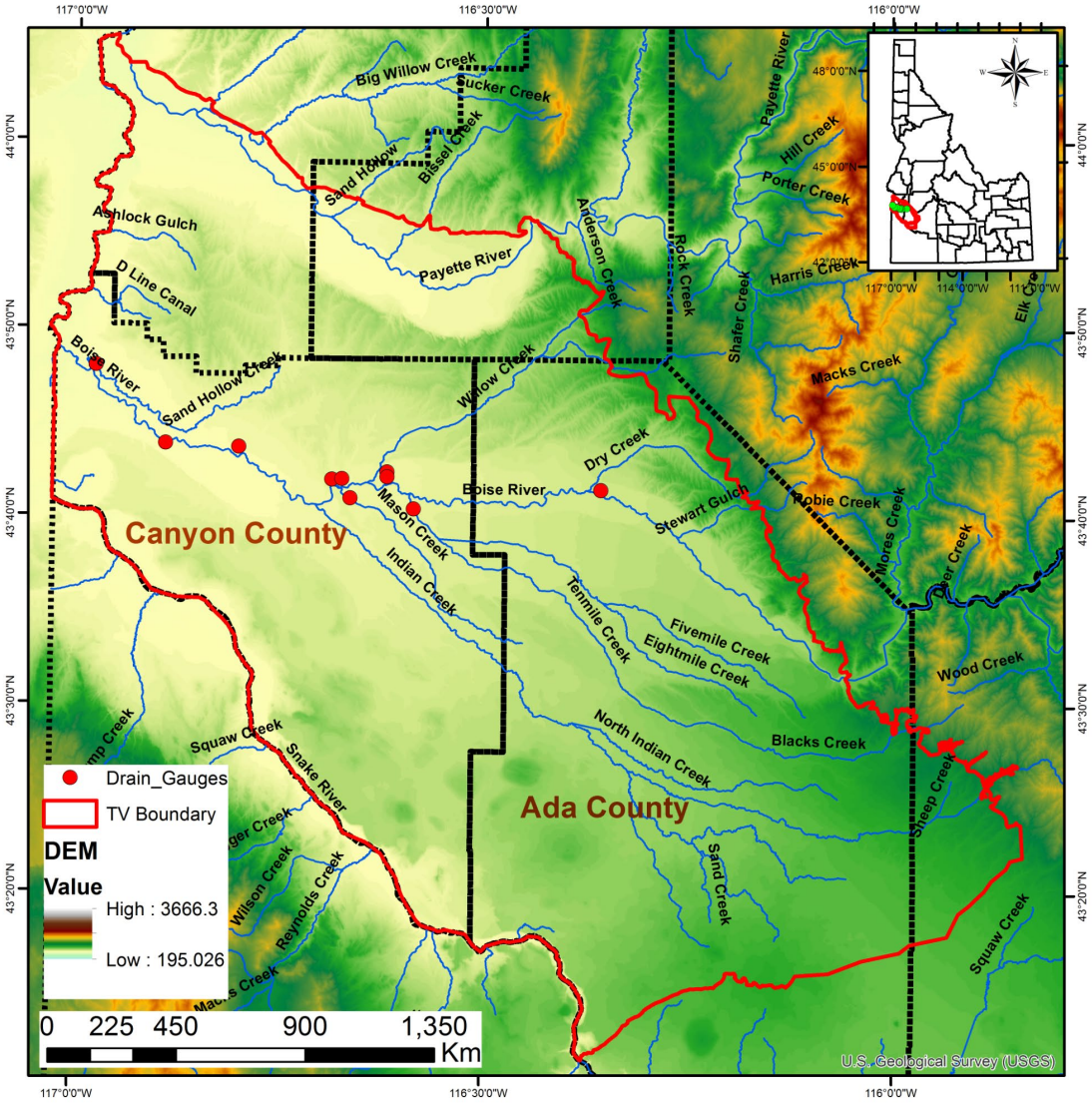


**Figure 1.1 Basemap for the study area**

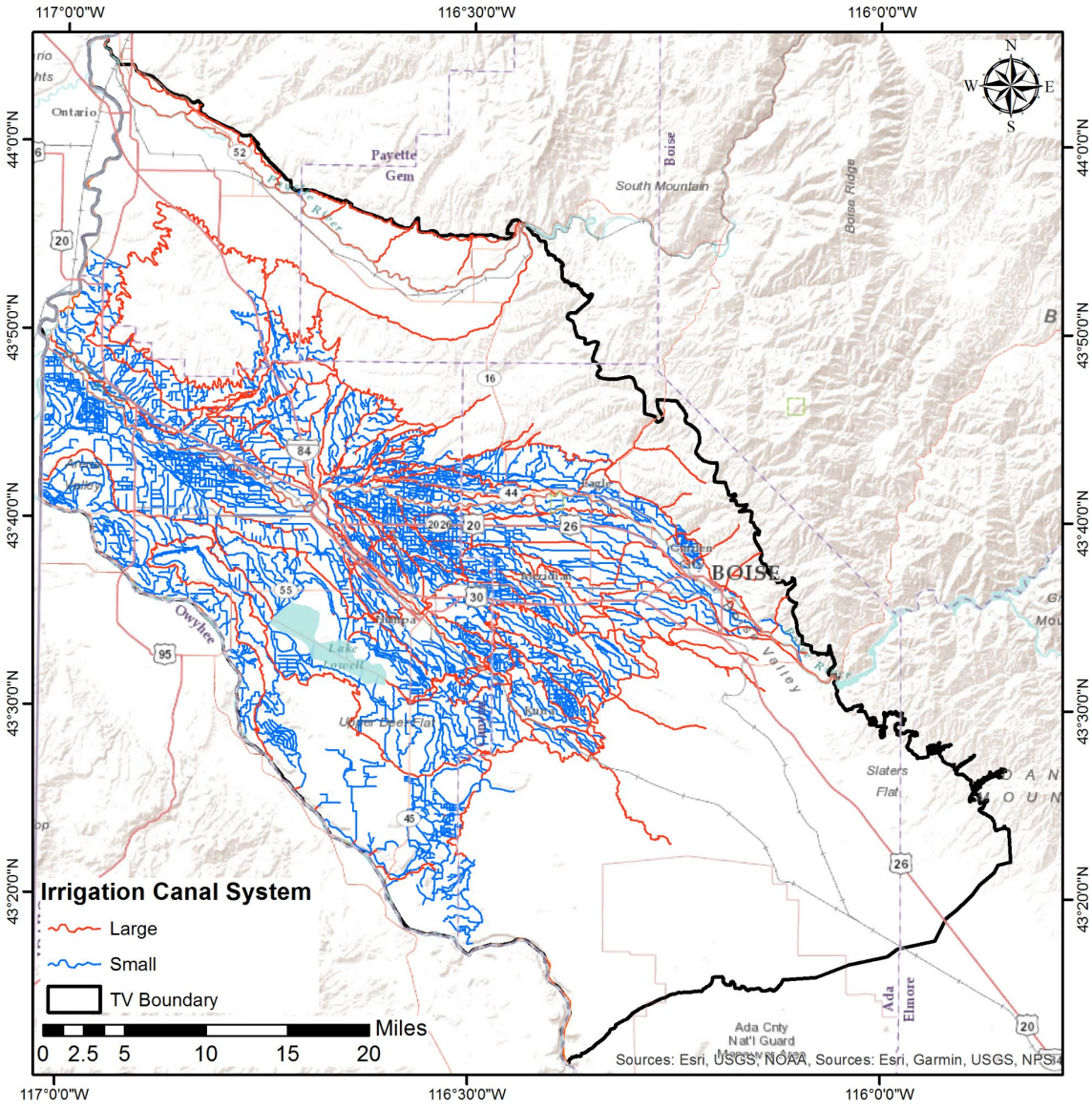


**Figure 1.2 Irrigation canals across the TV**

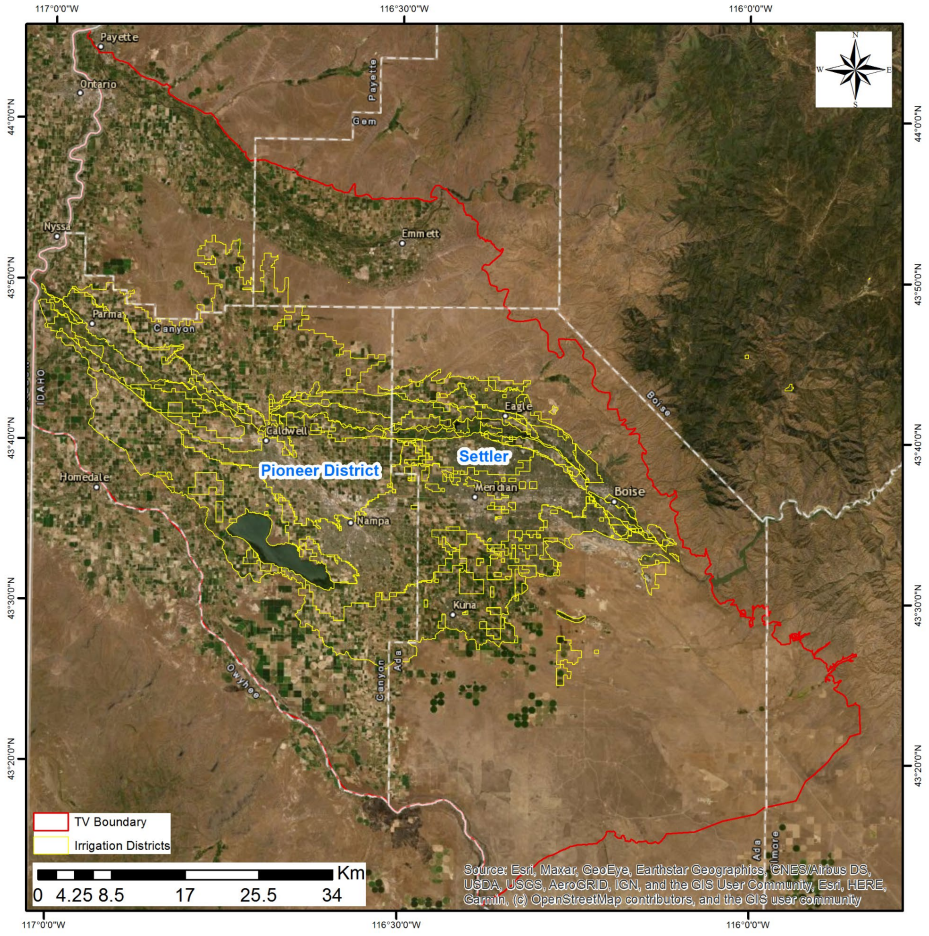


**Figure 1.3 Irrigation districts in the TV**

Flood irrigation in the early 1900s increased the shallow groundwater table in the TV, but with increasing irrigation efficiencies, they have been declining since the 1960s with a mean decline rate of about 2.9-3.9x10^-9 (m/s) (Contor et al., 2011). This technological advancement, which decreases water inefficiencies, has caused the rate of withdrawals to exceed the potential aquifer recharge rate. The intersection of various aquifer management activities needs to be addressed to evaluate how much incidental recharge is occurring across the basin, and to what degree this would further impact groundwater levels.

## 1.3 Geologic Context

In general, the lithological units in the TV contain granodiorite and granite (Kg), Basalts (Tpmb) and (QTb) of different epochs, and sedimentary rocks (Lewis et al., 2012). These sedimentary rocks, represented as fluvial and lake sediment (Qs), Lake Bonneville deposits (Qbs), landslide deposits (Qls), alluvial-fan (Qaf) and alluvial deposits (Qa), sometimes are found associated with either flood basalt (Tms) or basin and range extension (QTpms), or sediments (QTs) (Figure 1.4).

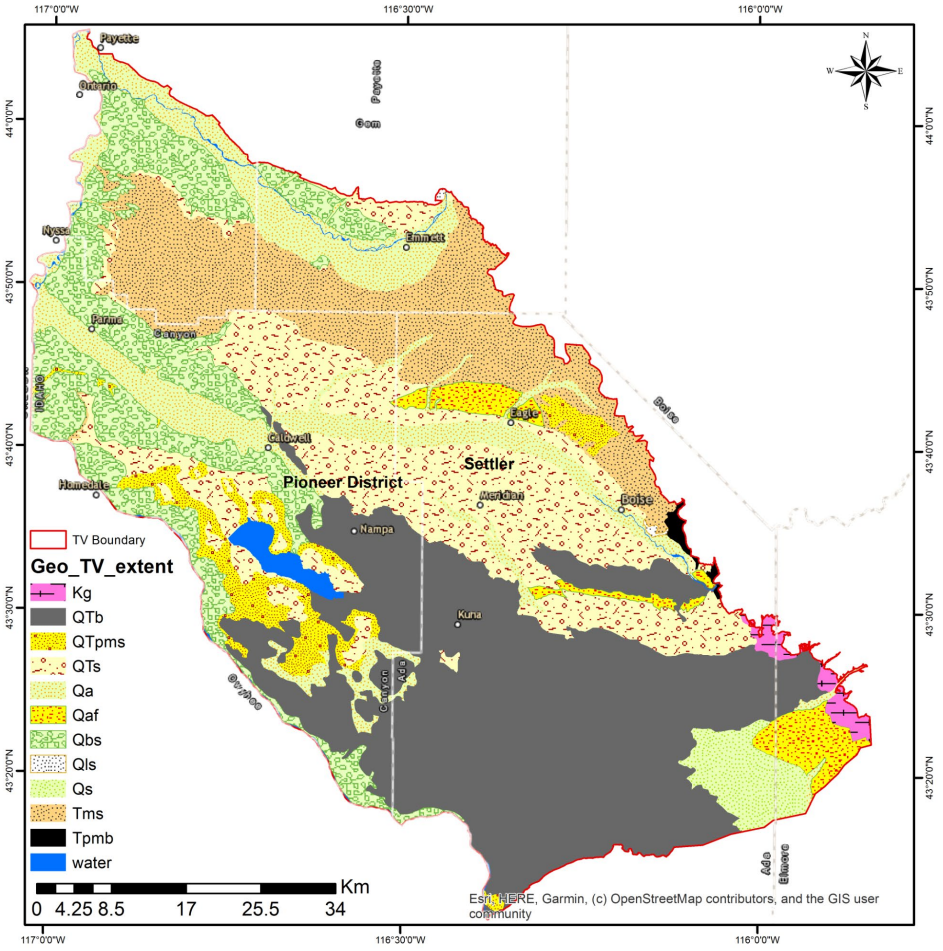


**Figure 1.4 Lithologic units covering the TV modified after (Lewis et al., 2012)**

The largest unit in the study area is basalt, covering approximately 1.42 x 10^9 m^2 which is 30.7% of the TV (4.63 x 10^9 m^2). The next largest units are sedimentary rocks which are associated with either sediments (QTs), or flood basalt (Tms), and Lake Bonneville deposits (Qbs) representing 19%, 14%, and 13% of the TV, respectively. The remaining 19% of the TV is covered by a combination of other units including alluvial, landslide, fluvial and lake sediment, sedimentary rocks with flood basalt, and granodiorite and granite.

In general, the sediments of this study area originated either by deposition, mass wasting, or floodplain deposition. The sources of basalt, granodiorite, and granite are basaltic volcanism, and magma cooling, respectively. Both alluvial and alluvial-fan deposits are mainly of gravel, sand, and silt including younger terrace deposits and/or some glacial deposits and colluvium in uplands. Landslide deposits are unsorted gravel, sand, and clay of landslide origin (including rotational and translational blocks and earth flows). Fluvial and lake sediments are fine-grained sediments with playa deposits of evaporative lakes in parts. Lake Bonneville deposits contain silt, clay, sand, and gravel deposited in and at margins of Lake Bonneville, and sand and gravel deposited in giant flood bars by outburst lake floods. Sedimentary rocks, associated with either basin and range extension or flood basalts, are fluvial and lacustrine deposits. These sedimentary rocks are found either with intercalated volcanic rocks of the Basin and Range Province, or associated with Columbia River Basalt Group and equivalent basalts for the latest unit (consolidated - weakly consolidated sandstones and/or siltstone, arkose, conglomerate, and clay). Sediments and sedimentary rocks are older gravel, sand, and silt of older terrace gravels. Basalt (Tpmb) and (QTb) are both olivine tholeiite basalt flows and cinder cones, but the

latter is covered by 1-3 m of loess. Granodiorite and granite contain biotite, commonly with muscovite.

### 1.4 Hydrogeologic Context

A hydrostratigraphic unit is "any soil or rock unit or zone which by virtue of its hydraulic properties has a distinct influence on the storage or movement of groundwater" (American Nuclear Society, 1980; Isensee et al., 1989). Generally, lithostratigraphic units are representatives of hydrogeologic units because a rock's lithology is affecting its hydraulic properties. The Snake River Plain, created in the middle Miocene as a graben-like structure, is subdivided into two major plains, the WSRP and eastern Snake River Plains (ESRP). Geology and hydrology of the WSRP are distinctly different from those of the ESRP; sedimentary rocks are dominant in the west while the east is commonly volcanic rocks (Newton, 1991). WSRP (northwest-trending plain), subsided relative to the surrounding area as a result of faulting triggered by volcanic activity, was then filled with river and lake deposits interbedded in places with basalt creating the current aquifer system underlying the TV and nearby vicinity (Bartolino and Vincent, 2017). Both plains are underlain by unconnected aquifer systems with a hydrologic boundary separating them near the King Hill area (Bartolino and Vincent, 2017). The SRP's subsurface geology below about 152.4 m, unlike surface geology, is generally poorly defined. However, the WSRP is commonly underlain by either unconsolidated and weakly consolidated Tertiary and Quaternary sedimentary rocks up to 1,524 m thick, or basalt which becomes more extensive in the vicinity of Mountain Home (Whitehead, 1992). Although most of the SRP regional aquifer system is dominated by the highly transmissive Quaternary basalt of the Snake River Group of permeable zones as a result of faults and fractures, coarse-grained

sedimentary deposits predominate the WSRP where their greatest thickness and transmissivity are along the northern margins, and decreases to the southwest, where lacustrine sedimentary are the dominant deposits (Whitehead, 1992).

Whitehead (1986, 1992) and Newton (1991) used a stratigraphic/lithologic approach to define the hydrogeologic units based on vertical variability, while Squires et al. (1992) and Wood (1997) use a depositional facies approach to account for horizontal and vertical variability. Whitehead (1986, 1992) described seven geologic units which form both the ESRP and WSRP aquifer systems, five of which are present in the WSRP, although Newton (1991) described only three major rock units forming the WSRP aquifer system. On the other hand, as one example of the facies approach, Squires et al. (1992) focused the top 304.8 m of the aquifer system sediments in the Boise area. The depositional facies guided them to define five different lithologic units of different hydrologic properties. In 2019, Bartolino combined these two approaches and defined four hydrogeologic units based on lithology. Stratigraphically, granitic and rhyolitic bedrock, fine-grained lacustrine deposits, Pliocene-Pleistocene and Miocene basalts, and coarse-grained fluvial and alluvial deposits are the four hydrogeologic units that were defined by Bartolino (2019). Generally, fine- and coarse-grained sediment are the main components of the aquifer's lower and upper portions, respectively. However, each hydrogeologic unit may significantly vary within itself. This variation increases with layer interbedding and interfingering, which in turn cause significant hydraulic properties variability over a short distance, either horizontally or vertically.

Fine-grained lacustrine deposits are the most extensive hydrogeologic unit in the WSRP aquifer system, while second, and third-largest units by volume are coarse-grained

fluvial and alluvial deposits, and Pliocene-Pleistocene basalts, respectively (Bartolino, 2019). However, coarse-grained fluvial and alluvial deposits are the source of most of the WSRP's wells due to its shallower depth compared to the fine-grained lacustrine deposits and rhyolitic and granitic basement, which are penetrated by fewer wells (Bartolino, 2019). Coarse-grained fluvial and alluvial deposits, commonly sands and gravels with interspersed finer-grained deposits, were deposited in two environments. Alluvial fans and stream deltas were deposited on the Chalk Hills Lake and Lake Idaho's northern and southern margins, and fluvial deposits were deposited on Lake Idaho's lacustrine sediments after the Snake River was formed and the lake drained (Bartolino, 2019). Pliocene-Pleistocene basalts interfinger with and are overlain by the two sedimentary hydrogeologic units because they erupted on land and within Lake Idaho, while Miocene basalts (of Columbia River Basalt Group) are overlain by the lacustrine, fluvial, and alluvial sediments and Pliocene-Pleistocene basalts (Bartolino, 2019). Fine-grained lacustrine deposits are clays and silts with some interspersed coarser-grains deposited in the Chalk Hills Lake and Lake Idaho, while rhyolitic and granitic bedrock mainly consist of Miocene rhyolites and other silicic volcanic rocks and Cretaceous granitic rocks of the Idaho batholith (Bartolino, 2019). Petrich and Urban (2004c) described the hydraulic connection between all of these units as "limited".

The Hydrogeologic setting in the TV (as a part of the WSRP) has been studied extensively by the USGS particularly through the Regional Aquifer-System Analysis (RASA) program, and the Idaho Department of Water Resources (IDWR), depth to water (Lindholm et al., 1982; 1986), irrigated lands and land use (Lindholm and Goodell, 1986), geohydrologic framework (Whitehead, 1986, 1992), transient and steady-state

MODFLOW models (Newton, 1991), and a water budget (Kjelstrom, 1995, Urban and Petrich, 1998, Urban, 2004). Groundwater and surface-water resources of the TV were reported by the Treasure Valley Hydrologic project (TVHP) including the hydrogeologic framework of Squires et al. (1992), and a groundwater-flow model by Petrich (2004a). SPF Water Engineering, LLC (2004), and Squires et al. (2007) provided information such as water levels, aquifer tests, groundwater-flow models, geophysics, and geochemical data on the Boise Valley-Payette Valley interfluve (the divide between the Boise and Payette Rivers). Groundwater occurrence and conditions were explained for some regions in the WSRP by Deick and Ralston (1986), Baldwin and Wicherski (1994), Tesch (2013), and Bartolino and Hopkins (2016). For instance, Deick and Ralston (1986) provided information on the groundwater resources in Payette County in the western edge of the WSRP which is a basin of lacustrine and fluvial deposits (mainly clay, sand and gravel) of more than 1219.2 m. Water levels had declined because recharge decreased as a result of four consecutive years of drought (Deick and Ralston, 1986). Baker (1991) concluded that there had been local declines in the potentiometric surface in the Dry Creek area, but these declines were minor compared to the saturated thickness of the entire aquifer system. The groundwater budget of WSRP has been examined by Kjelstrom (1995), Urban (2004), Schmidt et al. (2008), Sukow (2012), Lindgren (1982) and Tesch (2013). Reach gain/loss studies have been done intermittently over the past 25 years (Kjelstrom (1995), Berenbrock (1999), and Williams (2011). The first gain/loss analysis on the Lower Boise River Basin occurred in 1996 and 1997 (Berenbrock, 1999), where he pointed to the need for additional seepage studies on not only the Boise River and the New York Canal, but also on the irrigation canals and creeks. Williams (2011) investigated the seasonal gain/loss of a 2.25

x10^4-meter urbanized reach of the Lower Boise River from November 2009 until August 2010; seepage runs were conducted via 11 subreaches. In the same timeframe, the groundwater hydraulic gradient was evaluated via shallow groundwater mini-piezometers adjacent to the river at low stream discharge in February and high stream discharge in May (Williams, 2011). This study showed that the reach had a net gain from groundwater in November and February (low stream discharges), and a net loss to it in August (moderately high stream discharge), while the finding was unclear in May (higher stream discharge). The gain/loss estimates through these subreaches were supported by the measured hydraulic head differentials between the GW-SW. Water moved from the aquifer to surface-water in February (low stream discharge), while there was variability during May (high stream discharge). All of these studies show high spatial and seasonal seepage variability which may be constrained by implementing additional seepage measurements.

Most aquifer experiments conducted to assess the aquifer system's hydraulic properties are included in reports such as SPF Water Engineering (2004) and Hydro Logic Inc (2008) and a list of aquifer tests performed in the TV is included in Petrich and Urban (2004c). The Pierce Gulch Sand is a moderately to highly productive aquifer system (Squires et al., 2007) yielding from approximately 63-126 liters per second. Squires et al. (2007) also reported that about 876-1,314 liters per second flow northwestward in a five-mile swath through this sand aquifer, based on estimated water levels in wells and derived aquifer transmissivity values. Soil hydraulic properties (i.e, hydraulic conductivity, transmissivity, storage capacity, infiltration capability, and groundwater flow rate) are greatly dependent on the medium pore size distribution which is affected by the soil grains shapes, arrangement, and packing. Generally, large pore spaces exist in unconsolidated,

coarse-grained sediments (ie, coarse sand, and gravel) resulting in more productive aquifers due to the high hydraulic conductivity, while low hydraulic conductivities are common in compacted fine-grained deposits (i.e, silts, and clays) causing groundwater flow barriers. Accurate estimation of hydraulic conductivity is hard due to samples collection and their shipping to a laboratory for analysis. Douglas (2007) developed a numerical GW flow model to simulate the groundwater flow conditions between the valleys of Boise and Payette Rivers where some wells were selected and pumped to simulate the aquifer test conditions. Transmissivity and storativity values for the aquifer system(s) were derived by analysing the transient time-drawdown data which was collected during several aquifer tests conducted by previous investigators and by Douglas (2007). Hydraulic conductivity values (K) for regions within the model domain where aquifer tests have not been done, were determined by analyzing the driller's logs; specific values are representative for certain lithologic units, and viaa trial-and-error model calibration process (Douglas, 2007).

Mayo et al. (1984), Hutchings and Petrich (2002a, 2002b), Thoma (2008), Busbee et al. (2009), Welhan (2012), and Hopkins (2013) reviewed groundwater flow and recharge geochemistry studies. Stevens studied public land surveys in 1867 and 1875 to describe the hydrological conditions of the Boise River and Five Mile, Ten Mile and Indian Creeks, as well as the development of the irrigation-induced drainage system (Bartolino, 2019). For the westernmost part of the WSRP aquifer system, Bartolino (2019) documented the development of an updated three-dimensional hydrogeological framework model (3D HFM) while considering a conceptual groundwater budget.

Most of the surface water in the TV is generated from snow, representing approximately 90% of the TV's water- which accumulates in the upper Boise basin at

higher elevations where the annual precipitation can be approximately 1.5 meters (IWRB, 2012). Seventy-seven percent of the total annual Boise River streamflow occurs in the March/July runoff season, while 23 % occurs from August-February (IWRB, 2012). The Treasure Valley Aquifer System (TVAS) underlies the lower Boise basin stretching downstream from Lucky Peak Dam to the confluence with the Snake River and is the key source of approximately 95% of the TV' drinking water (IWRB, 2012).

The TVAS has a complex dynamic hydrologic interconnection of a deep, regional aquifer system (typically confined where water level is exceeding the water bearing zone depth, and of 76 to > 457 meter in depth), intermediate, and a shallow aquifer system (unconfined aquifer where depth to water table is the saturated zone's upper surface controlled by the local topography such as the canals' elevations, and of < 76 meter in depth). Topography, geologic faulting, and land use features such as local historic flood irrigation, control spatial variation in the aquifers' depths and thicknesses (IWRB, 2012). The hydraulic connection variability within this system increases the complexity of the dynamic hydrologic interconnection of the TVAS particularly in the aquifers underlying Boise foothills- Payette River and Mountain Home Plateau. The shallow aquifer (may contain local perched aquifers) is in direct hydraulic connection with surface water supplies. However, the hydraulic connection between surface water and either the intermediate or the deeper aquifers is limited (IWRB, 2012). Water exchange between surface and groundwater systems occurs first via the shallow zones, while the subsurface flow between both shallow and deeper regional aquifers have not been quantified (Urban, 2004). Both local hydraulic gradients and the aquifer's hydraulic characteristics are controlling the recharge to the deeper regional system.

## 1.5 Thesis Organization

This study addresses the complexity of GW-SW interactions in a semi-arid environment, where additional information on canal seepage variability and water flow measurement uncertainty is needed to better manage our existing water resources. Quantifying the variability of canal seepage is a significant knowledge gap in the TV's water budget. Our goal is to quantify the magnitude of seepage across the entire TV using the gain/loss method. This is accomplished by quantifying how much water is being exchanged between the shallow GW aquifer and SW in irrigation canals, testing and understanding how the canal characteristics (i.e., size and underlying lithology) and flow measurement uncertainty analyses affect the estimate of seepage which in turn is scaled to get the total TV's gain/loss. This seepage study is then integrated with DC Resistivity geophysical methods to provide additional information on seepage estimation and subsurface complexity of the basalt system. Specific findings of this thesis will be discussed in the following chapters.

Chapter 2 provides a detailed seepage study implemented across selected canal reaches of specific sizes and underlying lithology in the TV to quantify the gain/loss across the valley based on actual flow measurements. To determine which reach property is the largest contributor in seepage uncertainty, an uncertainty analysis is completed and to narrow down the number of measurements needed to be implemented using the DC Resistivity method (Chapter 3). The total gain/loss across the entire TV is then calculated by scaling the discrete measurements using 3 different scaling approaches. Seepage estimates using these scaling methods are then compared to estimates of previous water budgets. Chapter 3 tests how hydrogeophysical investigation may be useful for monitoring

SW-GW interactions in managed water resource systems. We accomplish this by first implementing a hydrogeophysical simulation using COMSOL Multiphysics and then DC resistivity measurements in the Basalt unit before and after the irrigation season starts to monitor the change of the subsurface saturation upon the water diversion in the irrigation canals. Finally, we provide additional insight into GW-SW interactions and water resources management by integrating between gain/loss method and DC resistivity method.

## References

American Nuclear Society, (1980). American national standard for evaluation of radionuclide transport in groundwater for nuclear power sites: La Grange Park, Illinois, ANSI/ANS-2.17-1980, American Nuclear Society.

Baker, S.J. (1991). Ground-water conditions in the Dry Creek area, Eagle, Idaho: Boise, Idaho Department of Water Resources Open-File Report, 27 p.

Baldwin, J. A., & Wicherski, B. (1994). Ground water and soils reconnaissance of the Lower Payette area, Payette County, Idaho.

Bartolino, J. R. (2019). Hydrogeologic framework of the Treasure Valley and surrounding area, Idaho and Oregon (No. 2019-5138). US Geological Survey.

Bartolino, J. R., & Hopkins, C. B. (2016). Ambient water quality in aquifers used for drinking-water supplies, Gem County, southwestern Idaho, 2015 (No. 2016-5170). US Geological Survey.

Bartolino, J. R., & Vincent, S. (2017). A groundwater-flow model for the Treasure Valley and surrounding area, Southwestern Idaho (No. 2017-3027). US Geological Survey.

Berenbrock, C. (1999). Streamflow Gains and Losses in the Lower Boise River Basin, Idaho, 1996-97. Water-Resources Investigations Report, 99, 4105.

Busbee, M. W., Kocar, B. D., & Benner, S. G. (2009). Irrigation produces elevated arsenic in the underlying groundwater of a semi-arid basin in Southwestern Idaho. Applied Geochemistry, 24(5), 843-859.

Contor, B., Farme, N., Moore, G., Owsle, D., Taylor, S., and Thiel, S. (2011). Managed Aquifer Recharge in the Treasure Valley: A Component of a Comprehensive Aquifer Management Plan and a Response to Climate Change. IWRRI Technical Completion Report 201102.

Cui, Y., & Shao, J. (2005). The role of ground water in arid/semiarid ecosystems, Northwest China. Groundwater, 43(4), 471-477.

Currell, M. J., Han, D., Chen, Z., & Cartwright, I. (2012). Sustainability of groundwater usage in northern China: dependence on palaeowaters and effects on water quality, quantity and ecosystem health. Hydrological Processes, 26(26), 4050-4066.

Dalin, C., Wada, Y., Kastner, T., & Puma, M. J. (2017). Groundwater depletion embedded in international food trade. Nature, 543(7647), 700-704.

Deick, J.F., & Ralston, D.R. (1986). Ground water resources in a portion of Payette County, Idaho: Moscow, Idaho Water Resources Institute, University of Idaho, 96 p.

Douglas, S. L. (2007). Development of a Numerical Ground Water Flow Model for the M3 Eagle Development Area Near Eagle, Idaho (Doctoral dissertation, University of Idaho).

Famiglietti, J. S. (2014). The global groundwater crisis. Nature Climate Change, 4(11), 945-948.

Hutchings, J., & Petrich, C. R. (2002a). Ground water recharge and flow in the regional treasure valley aquifer system: geochemistry and isotope study. Idaho Water Resources Research Institute.

Hutchings, J., & Petrich, C. R. (2002). Influence of Canal Seepage on Aquifer Recharge near the New York Canal. Idaho Water Resources Research Institute.

Hydro Logic Inc, (2008). Reanalysis of 16 aquifer tests in the greater Eagle-Star area of north Ada County, Idaho: Boise, Hydro Logic Inc., July 4, 2008, 256 p., 4 app.

Idaho Department of Water Resources, (1997). Map and GIS database: Boise Valley Project, Land Use and Land Cover, 1994. Based on 1:12,000 scale CIR photography. Map scale: 1:100,000.

Idaho Water Resources Board (IWRB), (2012). Proposed Treasure Valley Comprehensive Aquifer Management Plan. 44 p.

Isensee, A. R., Johnson, L., Thornhill, J., Nicholson, T. J., Meyer, G., Vecchioli, J., & Laney, R. (1989). Subsurface-water flow and solute transport: federal glossary of selected terms. US Geological Survey.

Jolly, I. D., McEwan, K. L., & Holland, K. L. (2008). A review of groundwater–surface water interactions in arid/semi-arid wetlands and the consequences of salinity for wetland ecology. *Ecohydrology: Ecosystems, Land and Water Process Interactions, Ecohydrogeomorphology*, *1*(1), 43-58.

Kemper, K. E. (2004). Groundwater—from development to management. Hydrogeology Journal, 12(1), 3-5.

Khan, H. H., Khan, A., Senapathi, V., Prasanna, M. V., & Chung, S. Y. (2019). Groundwater and surface water interaction. In GIS and Geostatistical Techniques for Groundwater Science, Edited by Senapathi Venkatramanan (pp. 197-207). Prasanna Mohan Viswanathan Sang Yong Chung, Elsevier.

Kjelstrom, L. C. (1995). Streamflow gains and losses in the Snake River and ground-water budgets for the Snake River Plain, Idaho and eastern Oregon (No. 1408-C).

Kumar, M. D. (2018). "Does Hard Evidence Matter in Policy Making? The Case of Climate Change and Land Use Change" in Water Policy Science and Politics (0-12-814903-5, 978-0-12-814903-4), (p. 99).

Lewis, R.S., Link, P.K., Stanford, L.R., & Long, S.P. (2012). Geologic map of Idaho: Moscow, Idaho Geological Survey M-9, scale 1:750,000, 1 sheet, 18 p. Booklet.

Lindgren, J.E. (1982). Application of a ground water model to the Boise Valley aquifer in Idaho: Moscow, University of Idaho, M.S. thesis.

Lindholm, G. F., Garabedian, S. P., Newton, G. D., & Whitehead, R. L. (1982). Configuration of the water table, March 1980, in the Snake River Plain regional aquifer system, Idaho and eastern Oregon (No. 82-1022).

Lindholm, G. F., Garabedian, S. P., Newton, G. D., & Whitehead, R. L. (1986). Configuration of the water table and depth to water, spring 1980, water-level fluctuations, and water movement in the Snake River Plain regional aquifer system, Idaho and eastern Oregon (No. 86-149).

Lindholm, G. F., & Goodell, S. A. (1986). Irrigated acreage and other land uses on the Snake River Plain, Idaho and eastern Oregon (No. 691). US Geological Survey.

Llamas, M. R., & Custodio, E. (Eds.). (2002). Intensive Use of Groundwater:: Challenges and Opportunities. CRC Press.

Malde, H. E. (1991). Quaternary geology and structural history of the Snake River Plain, Idaho and Oregon. The Geology of North America, 2, 251-281.

Mayo, A. L., Muller, A. B., & Mitchell, J. C. (1984). Geothermal investigation in Idaho. Part 14. Geochemical and isotopic investigations of thermal water occurrences of the Boise Front Area, Ada County, Idaho (No. DOE/ET/28407-T5). Idaho Dept. of Water Resources, Boise (USA).

Newton, G. D. (1991). Geohydrology of the regional aquifer system, western Snake River Plain, southwestern Idaho (Vol. 1408). US Government Printing Office.

Petrich, C.R. (2004a). Simulation of ground water flow in the lower Boise River Basin: Boise, University of Idaho, Idaho Water Resources Research Institute Research Report IWWRRI-2004-02, 130 p.

Petrich, C.R. (2004b). Treasure Valley Hydrologic Project executive summary: Moscow, University of Idaho Water Resources Research Institute, Research Report IWRRI-2004-04, 33 p.

Petrich, C.R. & Urban, S.M. (2004c). Characterization of ground water flow in the lower Boise River basin: Moscow, University of Idaho Water Resources Research Institute, Research Report IWRRI-2004-01, 149 p.

Rodell, M., Famiglietti, J. S., Wiese, D. N., Reager, J. T., Beaudoing, H. K., Landerer, F. W., & Lo, M. H. (2018). Emerging trends in global freshwater availability. Nature, 557(7707), 651-659.

Schmidt, R.D., Cook, Z., Dyke, D., Goyal, S., McGown, M., & Tarbet, K. (2008). Distributed parameter water budget data base for the lower Boise Valley—U.S. Bureau of Reclamation. Pacific Northwest Region, 109 p.

Squires, E., Utting, M., & Pearson, L. (2007). M3 Eagle regional hydrogeologic characterization, North Ada, Canyon, and Gem Counties, Idaho, year one progress report—May 4, 2007: Boise, Idaho, Hydro Logic, Inc., consultants' report, 31 p.

Squires, E., Wood, S.H., & Osiensky, J.L. (1992). Hydrogeologic framework of the Boise aquifer system, Ada County, Idaho: Moscow, University of Idaho, Idaho Water Resources Research Institute Research Technical Completion Report 14-08-0001-G1559-06, reprinted with corrections, 75 p.

Sukow, J. (2012). Expansion of Treasure Valley Hydrologic Project groundwater model: Boise, Idaho Department of Water Resources, 34 p.

Tesch, C. (2013). East Ada County comprehensive hydrologic investigation: Boise, Idaho Department of Water Resources Technical Report, 51 p.

Thoma, M. (2008). Investigating recharge routes to the Treasure Valley Aquifer System, Idaho using noble gas thermometry: Boise, Boise State University M.S. Thesis, 400 p.

Urban, S.M. (2004). Water budget for the Treasure Valley aquifer system for the years 1996 and 2000: Moscow, University of Idaho Water Resources Research Institute, Research Report unnumbered, variously paged.

Urban, S.M. & Petrich, C.R. (1998). 1996 water budget for the Treasure Valley aquifer system. Treasure Valley Hydrologic Project Research Report, Idaho Department of Water Resources, Boise, Idaho.

U.S. Board on Geographic Names, (2019). U.S. Board on Geographic Names: U.S. Geological Survey website, accessed May 20, 2019, at https://www.usgs.gov/core-science- systems/ ngp/ board- on- geographic- names]

Vrba, J., & Renaud, F. G. (2016). Overview of groundwater for emergency use and human security. Hydrogeology Journal, 24(2), 273-276.

Water Engineering, S.P.F. (2004). Aquifer evaluation in the Big Gulch and Little Gulch areas of Spring Valley Ranch: Boise, Idaho, SPF Water Engineering, LLC, Report prepared for SunCor Development Company, 23 p., 6 apps.

Welhan, J.A. (2012). Preliminary hydrogeologic analysis of the Mayfield area, Ada and Elmore Counties, Idaho: February, 42 p.

Whitehead, R.L. (1986). Geohydrologic framework of the Snake River Plain, Idaho and eastern Oregon: U.S. Geological Survey Open-File Report 87–107, 60 p.

Whitehead, R.L. (1992). Geohydrologic framework of the Snake River Plain regional aquifer system, Idaho and eastern Oregon: U.S. Geological Survey Professional Paper 1408-B, 32 p., 6 plates in pocket.

Williams, M. L. (2011). Seasonal Seepage Investigation on an Urbanized Reach of the Lower Boise River, Southwestern Idaho, Water Year 2010 (No. 2011-5181). US Geological Survey.

Winter, T. C., Harvey, J. W., Franke, O. L., & Alley, W. M. (1998). Ground water and surface water: a single resource (Vol. 1139). US geological Survey.

Wood, S.H. (1997). Structure contour map of top of the mudstone facies, western Snake River Plain, Idaho: Boise State University, Contribution to the Treasure Valley Hydrologic Project, 1 sheet, scale 1:100,000.

# CHAPTER 2: CHARACTERIZING GROUNDWATER-SURFACE WATER EXCHANGE IN IRRIGATION CANALS VIA GAIN LOSS METHOD

## 2.1 Background and theory

### 2.1.1 Canal Seepage

Many kilometers of irrigation canals are passing through the TV; about 1,882,932 m of larger canals (IDWR, 1997) and many kilometers of smaller canals and ditches exist within the valley. These mapped canals are shown in Figure 1.2. The unknown spatial distribution and total length of the smaller canals are the reasons for not getting precise seepage estimation because most of them have not been mapped (Urban, 2004). Estimating the seepage rate is essential for water budget evaluation because it represents a key source of groundwater recharge (Urban, 2004).

In general, groundwater inflows and outflows are the main components of the mass balance equation in the TV aquifer system, where the inflows into this system involve seepage from canals, rivers and streams, Lake Lowell, and from rural domestic septic systems, underflow, and infiltration of precipitation and surface water used for irrigation. Outflows include municipal, industrial, irrigation, rural domestic, and stock withdrawals, discharge to canals, drains, and rivers, and evapotranspiration (ET) (Urban, 2004).

$$Inflows - Outflows = \frac{ds}{dt} \qquad (2.1)$$

Where $\frac{ds}{dt}$ is the instantaneous change in aquifer storage with respect to time.

Recharge and withdrawal areas do not match throughout the valley. Zones with extensive canals and/or flood irrigation are recharge areas, while the greatest withdrawal sites exist where there is no surface water irrigation (Urban, 2004). Consequently, withdrawals within the TV in local areas may exceed the recharge causing local water levels' declining, while water levels' increasing may be observed in areas where the recharge exceeds local withdrawals.

To assess seepage, flow is determined over a short time interval at several locations along canal reaches. These measurements allow groundwater runoff assessment (how much exists and what the origin is) and afford indications to the basin geology (Cheremisinoff, 1998). For instance, gaining reaches may be indications for high permeable zones containing sand and gravel deposits, fractures, limestone solution openings (Cheremisinoff, 1998). These gaining reaches may also indicate increased permeability in or close to the stream channel because of local facies changes. This may cause groundwater to discharge through springs and seeps, along valley walls or the stream channel, or seep directly upward into the stream (Cheremisinoff, 1998).

Throughout those measurements, it is important that there is no surface runoff. Generally, most researchers prefer seepage studies during periods when the flow rate is sufficiently small that it is equalled or exceeded 90 percent of the time. Streamflow data may provide a way for checking groundwater system estimates in areas where the geology and groundwater systems are not well understood.

The positive net differences in aquifer storage between the total inflows and outflows for 1996 and 2000 are 7,300 af. and 88,600 af, respectively (Urban, 2004). The surplus groundwater is concealed by the error margin related to some water budget factors

and most of the difference between both values may be assigned to components' estimation mechanisms (Urban, 2004).

Water budgets for the WSRP including the TV area were compiled by Newton (1991) and Kjelstrom (1995). A groundwater model of the WSRP was presented in coincidence with Newton's (1991) water budget. Newton (1991) reported that there was a large uncertainty range related to the water budget since certain component values could not be clearly outlined such as the return flow amount attributed to groundwater discharge. Surface water irrigation represented 80% of groundwater inflows (Newton, 1991), while approximately 83% of groundwater outflows was directed to rivers and drains. The majority of groundwater discharges are to rivers and drains, mainly during the irrigation season (Kjelstrom, 1995). Groundwater storage increased by approximately 3 million af through the 1930 to 1972 time period, while it generally decreased over the 1972 to 1980 period. Several gain and loss short-term cycles during the 1930 to 1980 period were observed. Kjelstrom (1995) assigned some of them to periods of above and below normal precipitation and he claimed that fluctuations in this storage are the result of 100 consecutive years of irrigation across the whole Snake River Plain.

The major source of inflows is seepage from the canal system, followed by seepage from flood irrigation and precipitation (Urban, 2004). Most recharge encounters the shallow aquifer only; recharge to the deeper aquifers is much less than to the shallow system (Petrich, 2004b). The research outlines the largest water budget component (i.e; the canal seepage).

## 2.2 Methods

### 2.2.1 Site Selection

The Pioneer Irrigation District was selected to take flow measurements across its canals as representatives to the TV because it was the irrigation district that was willing to collaborate with us to do this seepage study. Pioneer District covers 1.4x10^8 sq. m. Geologically, this district is dominated by multiple lithological units (Lewis et al., 2012) (Figure 2.1). These lithologic units are sediments and sedimentary rocks (QTs) which are represented by older gravel, sand, and silt; Lake Bonneville deposits (Qbs) which generally consist of silt, clay, sand, and gravel; Basalt (QTb) which is flows and cinder cones of olivine tholeiite basalt; Alluvial deposits (Qa) consisting of gravel, sand, and silt, and sedimentary rocks associated with Basin and Range extension (QTpms) of fluvial fan and lacustrine deposits and intercalated volcanic rocks of the Basin and Range Province (Figure 2.1). These lithologic units cover areas of approximately 74.3 (52%), 40.7 (28.6%), 19.96 (14%), 6.7 (5%), and 0.8 (0.57%) square kilometers of Pioneer District, respectively. Six canal reaches were selected to represent the major three lithological units covering this area; two reaches of different sizes in each of QTs, Qbs, and QTb lithological units. Fivemile Feeder (5.5 m wide) and 5.17 Lateral (3.5 m wide) were selected in the QTs unit where the major sediments are Gravel, Sand, and Silt, Indian Creek (4.3 m wide) and 15.0 Lateral of (3.06 m wide) were chosen to represent QTb where the dominant rock is Olivine basalt to represent the relatively larger and smaller canals, respectively. Two reaches of the Phyllis canal; Phyllis R1 (3.01 m wide) and Phyllis R2 (2.87 m wide) were selected in Qbs where the dominant sediments are gravel, sand, silt, and clay.

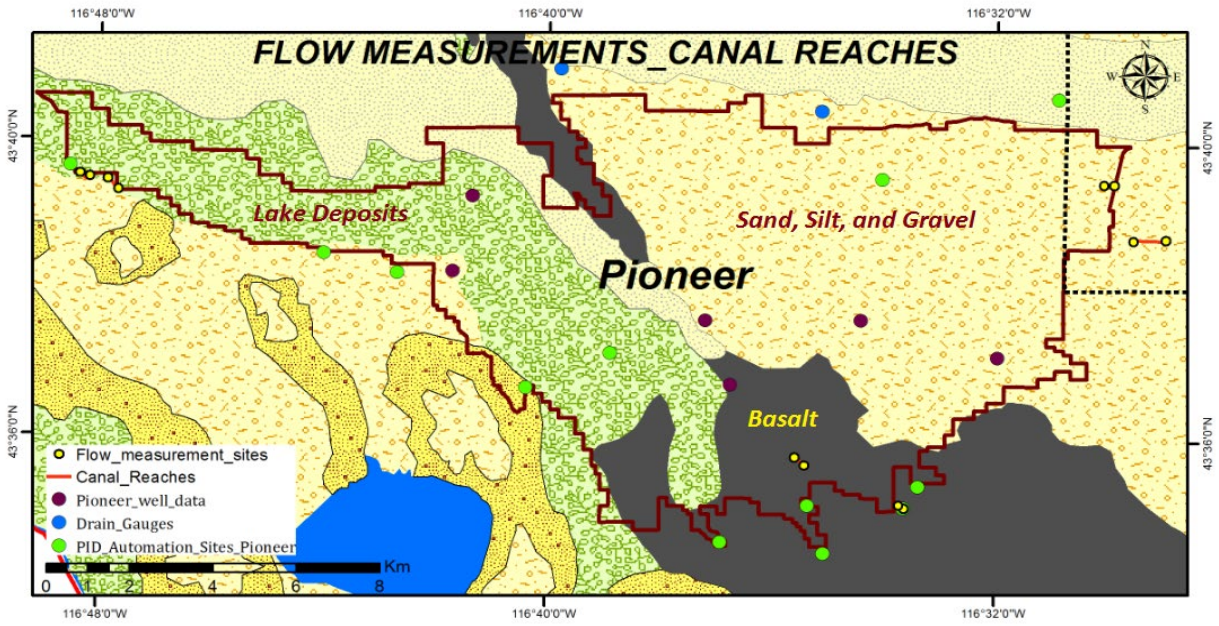


**Figure 2.1 Lithologic map for Pioneer district modified after (Lewis et al, 2012)**

2.2.2 Gain Loss Method

A gain/loss method quantifies net channel losses or gains of water between surface water and the shallow groundwater aquifer systems over a given time. Collecting streamflow measurements along the main channel of a reach is the traditional procedure of gain-loss analysis (Slade et al., 2002). Channel gain or loss can be computed for each reach by equating inflows to outflows plus flow gain or loss in the reach (Slade et al., 2002):

$$Qu + Qt + Qr = Qd + Qw + Qe + Qg \qquad (2.2)$$

Where Qu is streamflow at the upstream end of the reach, Qt is streamflow from tributaries into the reach, Qr is return flows to the reach, Qd streamflow at the downstream end of the reach, Qw is withdrawals from the reach, Qe is evapotranspiration from the reach, and Qg is either gain (positive) or loss (negative) in reach.

Thus,

$$Q_g = Q_u + Q_t + Q_r + Q_d + Q_w + Q_e \qquad (2.3)$$

To determine how much water is being lost from or entering these canal reaches, flow measurements were collected during July and August 2020 through these canals using a Marsh Mcbirney Flow Meter. At the upstream and downstream transects, the velocities of flows were measured at 60% of the depth (from the top) and the recorded velocity was used as the mean velocity at each width interval along the cross section (Photo 2.1). If the depth exceeded 0.81 m, two flow velocity measurements were recorded at 20% and 80% of the depth (from the top) and the average of the two velocities were used as the mean velocity. These flow measurements were taken at the upstream and downstream ends of each canal reach weekly over six weeks. The total cross-sectional discharges for all reaches were calculated using the following equation (except for the discharge at the downstream cross-section of the Fivemile feeder):

$$\boldsymbol{Q = 0.0283 \sum_{i=1}^{n} v_i w_i d_i} \qquad \boldsymbol{(2.4)}$$

where Q is discharge (cubic meter per second (cms)), v is velocity (m/s), w is width (m), and d is depth (m).

Underflow (flow parallel to stream through shallow channel-bed deposits) and bank storage are considered negligible or minimal and Qr is assumed to be zero. Although the flow measurements were done during the Summer in July and August, evapotranspiration is assumed to be negligible because of the short durations of the measurements, and the short length and width of the canal reaches that would allow only minimal

evapotranspiration losses. So, Qe is assumed to be zero. In gain-loss studies, it is essential to detect and measure the discharge for all withdrawals, flowing tributaries, and return flows to be included in the calculation of the reach gain or loss. However, attempts were made to avoid having any inflows or outflows sources for the reaches in this study. Therefore, Qt and Qw are assumed to be zero. As a result, for determining the gain/loss Qg through each reach, the differences between the total discharge at the upstream Qu and that at the downstream Qd cross sections were calculated for each reach weekly.

**Photo 2.1 Flow measurements at 15 Lateral, Fivemile Feeder, and Indian Creek, from left to right.**

Stream bed conditions made it not possible to take measurements at the downstream section of the Fivemile feeder, so water depth was measured at the weir at the downstream of this reach. Discharge was calculated using the following equation created by the Pioneer District (provided by personal communication with Kirk Meyers):

$$Q = AD^B \qquad (2.5)$$

where the coefficient A = **47.331,** D is the depth in ft, and exponent (B) =**1.5135**. The rating curve coefficient and exponent are difficult to convert to SI metric units because this equation is an empirical relationship and the coefficient and exponent have units embedded to them. So, the input in this equation is in feet and the output is in cubic feet per second.

2.2.3 Uncertainty Analysis

Several previous studies have focused on the uncertainty estimation of streamflow measurements by the velocity area method (i.e., direct discharge) such as Pelletier (1988), Sauer and Meyer (1992), and Boning (1992). These uncertainty estimates of the individual measurements of streamflow in ideal, average, and poor conditions were summarized by Harmel et al. (2006). Generally, these estimates are ranging from ±2% and ±20% for the ideal and poor conditions, respectively (Harmel et al., 2006). Harmel and others presented the potential uncertainty of the streamflow data resulting from cumulative errors created during the individual streamflow measurements, stage-discharge relationship, continuous stage measurement, and the variability of the stage measurement due to streambed characteristics. They estimated the streamflow probable error (EP) as 42% in the worst scenario while varying from 6% to 19% in the typical conditions.

Uncertainty estimation is important, particularly through canal locations with minimal seepage rates. To calculate the uncertainty related to the measurements we used a Monte Carlo approach, making assumptions about the sources and magnitude of measurement errors and then propagating those errors through the above calculations. The accuracy of the velocity measurement was assumed to be ± 3% of reading, while the width and depth errors were assumed to be 0.03 m and 0.025 m, respectively. The width and depth errors are treated as Additive White Gaussian (AWG), while the velocity error is treated as a multiplicative error. Given these assumptions, normally distributed random numbers for each of the two variables (width and depth) were created, while the velocity error was uniformly distributed. Except for the downstream section of the Fivemile feeder, these assumptions were used to quantify the uncertainty of both upstream and downstream discharges for all canal reaches. The measurements of width, depth, and flow velocity were perturbed 5000 times using the assumed errors characteristics above and the upstream and downstream flow rates calculated.

### 2.2.4 Scaling

The discrete flow measurements, made through canal reaches of different characteristics, were scaled using three different approaches to estimate the total seepage across the whole TV (Figure 2.2) while taking into account the measurement uncertainty. The simplest approach (Method A`) simply scaled the measurements evenly through the entire length without considering the canal characteristics. The 2020 irrigation season lasted for 198 days (April 1st to October 15th) (personal communication, Kirk Meyers). Although there might be some losses during the remainder of the year, we were interested in the irrigation season in particular given the associated impact on water rights. Since the

canal size and lithology significantly affect canal seepage, two other approaches were used in scaling the canal seepage measurements. Method B‵ considers the lithologic difference of the 3 key units covering the TV, and Method C‵ also includes canal size, where the length of each canal size in each lithologic unit was calculated from the TV's irrigation canal system provided by the IDWR.

The conceptual diagram (Figure 2.2) and the following equations demonstrate how we got G/L over the major three units of the TV.

Method A:

$$Mean\ (\frac{cfs}{mi_r}) = \frac{\frac{\sum\ G/L}{n_{reaches}}}{L_{reaches}} \qquad (2.6)$$

$$Total\ G/L\ (\frac{acre.ft}{yr}) = Mean\ (\frac{cfs}{mi_r})\ L_{canals}\ x\ 392.7\ (\frac{acer.ft}{yr}) \qquad (2.7)$$

Method B:

$$Mean\ (\frac{cfs}{mi_{r.Lithn}}) = \frac{\frac{\sum\ G/L}{n_{r.Lithn}}}{L_{r.Lithn}} \qquad (2.8)$$

$$Total\ G/L\ (\frac{acre.ft}{yr})$$

$$= \sum \quad Mean\ (\frac{cfs}{mi_{r.Lithn}})\ x\ L_{canals.Lithn}\ x\ 392.7\ (\frac{acer.ft}{yr}) \quad (2.9)$$

Method C:

$$Mean\ (\frac{cfs}{mi_{r.Sn.Lithn}}) = \frac{\frac{\sum \quad G/L}{n_{r.Sn..Lithn}}}{L_{r.Sn..Lithn}} \qquad (2.10)$$

$$Total\ G/L\ (\frac{acre.ft}{yr})$$

$$= \sum \quad Mean\ (\frac{cfs}{mi_{r.Sn.Lithn}})\ x\ L_{canals.Sn.Lithn}\ x\ 392.7\ (\frac{acer.ft}{yr}) \qquad (2.11)$$

Where G/L is gain/loss, cfs is cubic feet per second, n is a number of (either reaches, lithologic units, or canal sizes), mi is mile, r is reach, L is length, Lith is lithologic unit, and S is canal size.

The measured canals were located in the major lithologic units that dominate the TV, so similar lithologic units were grouped together and added to the most similar unit of the major lithologic units to obtain the total G/L for the entire TV (Appendix A3). Small canals refer to small supplies and drains, while large canals refer to anything else other than the rivers, creeks, and Lake Lowell. These calculations were performed using only the TV's GW flow model extent (provided by personnel communication with Stephen Hundt) for Idaho, ignoring the small extent of the TV in Oregon.

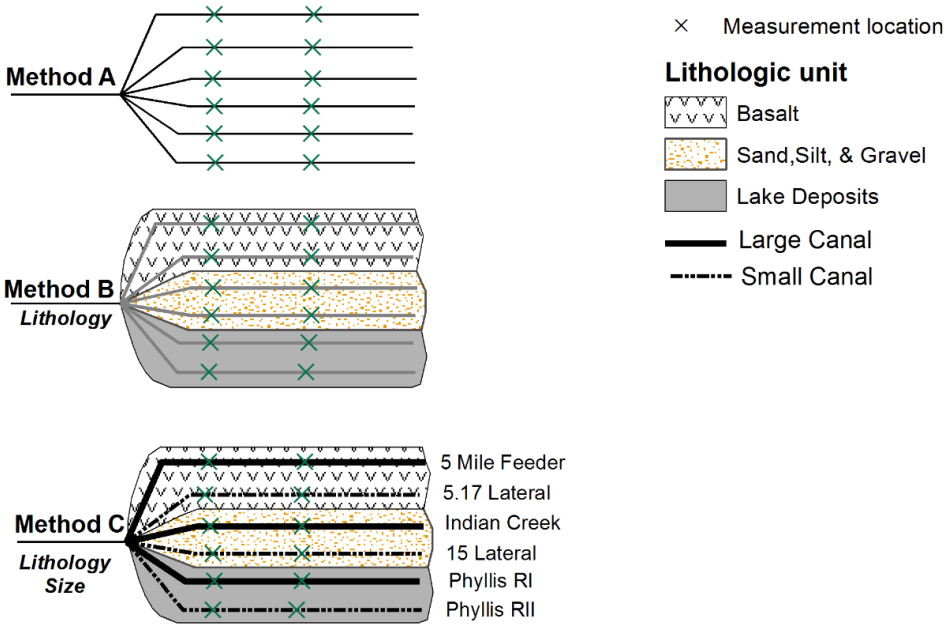


**Figure 2.2 A conceptual diagram shows 3 different approaches of scaling to get the total G/L across the TV**

## 2.3 Results

A time series-plot of the gain/loss in cfs for the six canals is shown in Figure (2.3). This figure shows that Fivemile feeder almost has a consistent behavior and is losing water each time with almost 0.42 cms, while Indian Creek, Phyllis R2, and 5.17 Lateral are fluctuating between losing and gaining and it is important to know if these behaviors are attributed to the uncertainty of our measurements or may be other controlling factors. So, the uncertainty analysis is essential to get a robust conclusion.

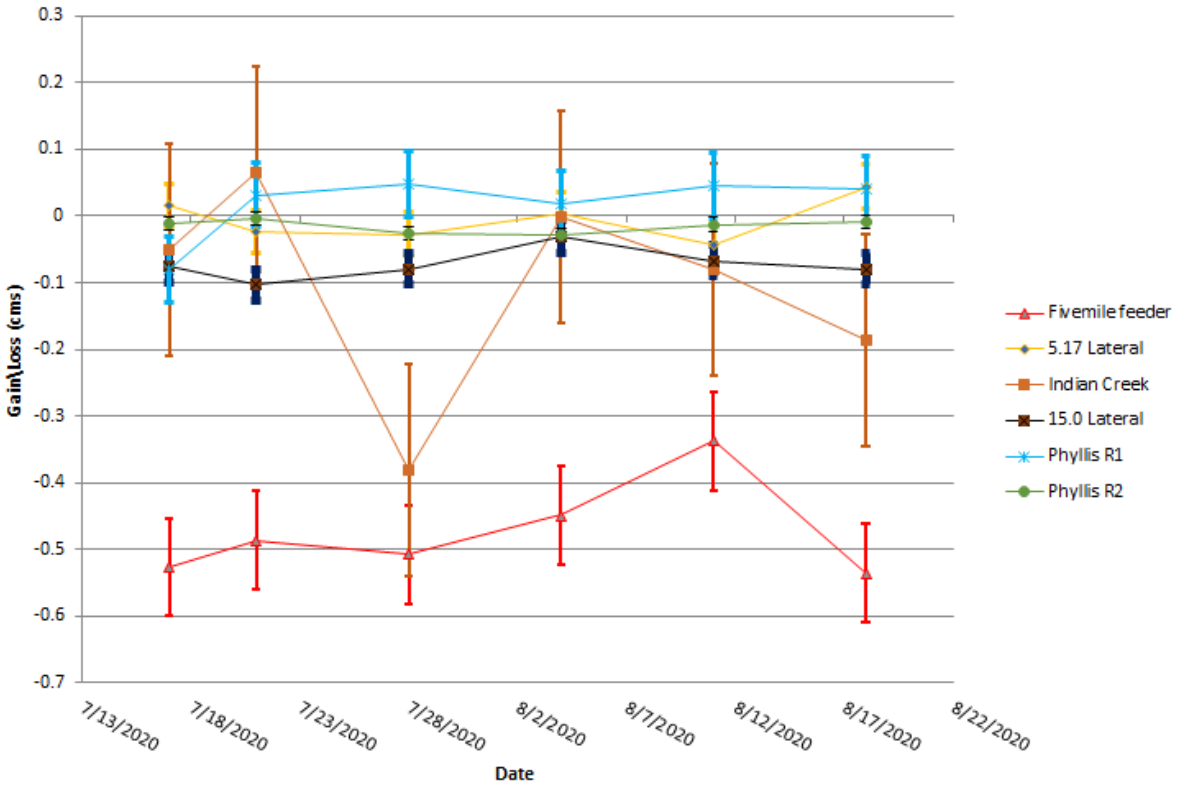


**Figure 2.3 Time series plot showing the gain/loss with error bars for the canals**

For each canal reach, the distribution of discharge was calculated for both the upstream and downstream cross sections (Appendix A1), and their gain/loss histograms were created (Figures 2.4:2.10) to show variability at each reach for each sampling date. Figure (2.11) shows variability across lithologic units. Uncertainty analysis of the discharge at downstream Fivemile feeder cross section is summarized in (Appendix A2). The means and standard deviations of the gains and losses of these reaches were used to test how the canal variability and water flow measurement uncertainty affect the magnitude of the seepage rate through each canal (Table 2.1). These uncertainty estimates were then used to evaluate total canal seepage across the whole TV. Properties of the measured canal reaches and their gain/loss average in cms are summarized in (Table 2.2)

**Table 2.1 Statistics of gains and losses of the canal reaches**

| | Unit Name | Sand, Silt, & Gravel Unit | | Basalt Unit | | Lake Deposits Unit | |
|---|---|---|---|---|---|---|---|
| Date | Reach Name | 5Mile feeder/ Method A | 5.17 Lateral | Indian Creek | 15 Lateral | Phyllis RI | Phyllis RII |
| | m^3/s | | | | | | |
| 07/17 | Mean G/L | -0.527 | 0.016 | -0.05 | -0.075 | -0.08 | -0.01 |
| | Std. | 0.088 | 0.006 | 0.008 | 0.075 | 0.0025 | 0.002 |
| 07/21 | Mean G/L | -0.487 | -0.024 | 0.065 | -0.1 | 0.03 | -0.003 |
| | Std. | 0.087 | 0.006 | 0.005 | 0.005 | 0.003 | 0.001 |
| 07/28 | Mean G/L | -0.51 | -0.027 | -0.38 | -0.079 | 0.047 | -0.026 |
| | Std. | 0.088 | 0.006 | 0.009 | 0.005 | 0.005 | 0.005 |
| 08/04 | Mean G/L | -0.45 | 0.004 | -0.0003 | -0.03 | 0.018 | -0.028 |
| | Std. | 0.087 | 0.006 | 0.007 | 0.005 | 0.005 | 0.005 |
| 08/11 | Mean G/L | -0.34 | -0.04 | -0.079 | -0.067 | 0.045 | -0.012 |
| | Std. | 0.088 | 0.006 | 0.006 | 0.004 | 0.005 | 0.004 |
| 08/18 | Mean G/L | -0.54 | 0.04 | -0.186 | -0.079 | 0.039 | -0.008 |

| | | | | | | | |
|---|---|---|---|---|---|---|---|
| | Std. | 0.088 | 0.005 | 0.009 | 0.005 | 0.006 | 0.007 |

**Table 2.2 Properties of the measured canal reaches and their gain/loss average in cubic meter per second (cms)**

| Lithologic Unit/ area (m^2) | Lithologic Unit | Name | Length (m) | Width _Mean (m) | Mean G/L (cms) |
|---|---|---|---|---|---|
| QTs (8.7 × 10^8) | Gravel, Sand, Silt | Fivemile Feeder | 798.2 | 5.45 | -0.43 |
| | | 5.17 Lateral | 234.96 | 3.5 | -5.18 × 10^-3 |
| QTb (4.09409 × 10^8) | Basalt | Indian Creek | 136.8 | 4.25 | -0.105 |
| | | 15 Lateral | 318.65 | 3.06 | -0.07 |
| Qbs (6.167306 × 10^8) | Lake Deposits | Phyllis R1 | 373.4 | 3.01 | 0.0169 |
| | | Phyllis R2 | 344.4 | 2.89 | -0.014 |
| Mean G/L in cms over all the six reaches | | | | | -0.1016 |

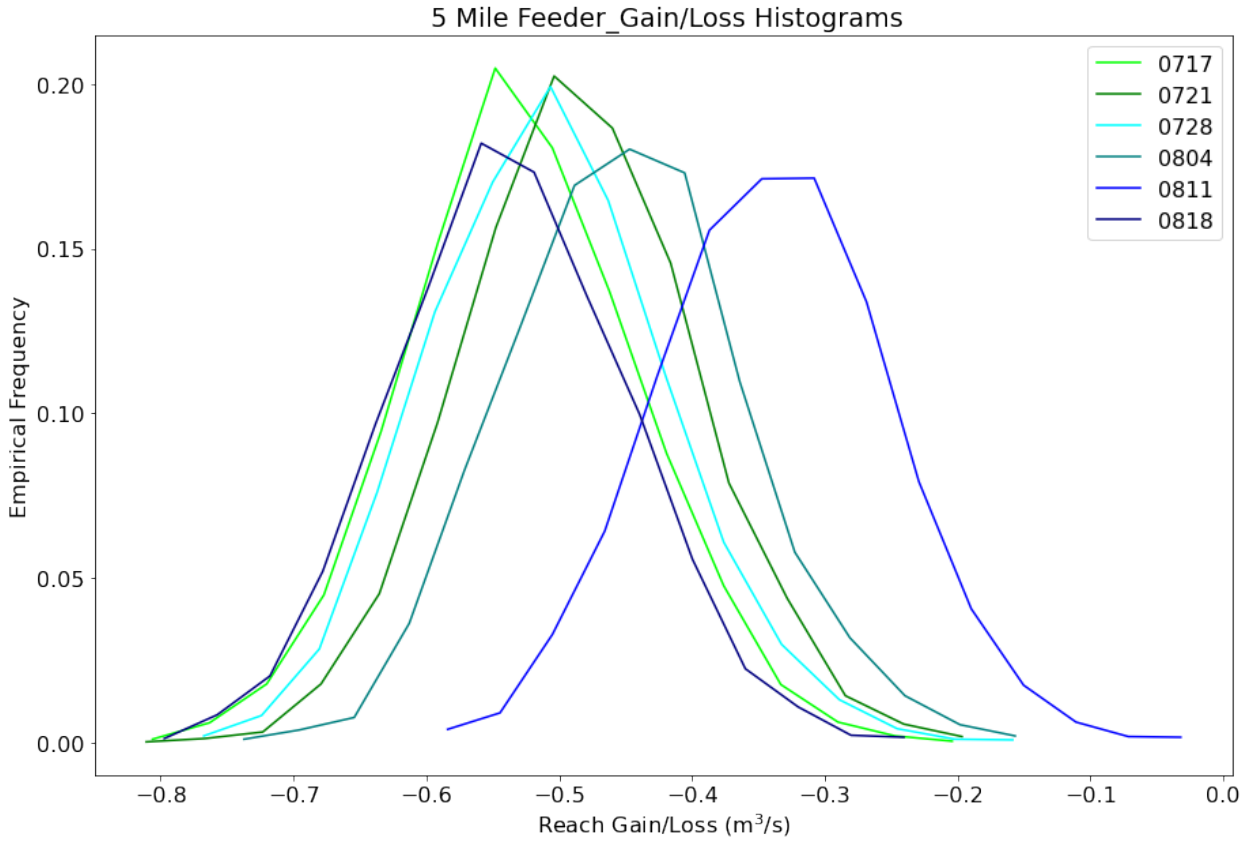


**Figure 2.4 G/L histograms for each sampling date showing variability at 5 Mile Feeder**

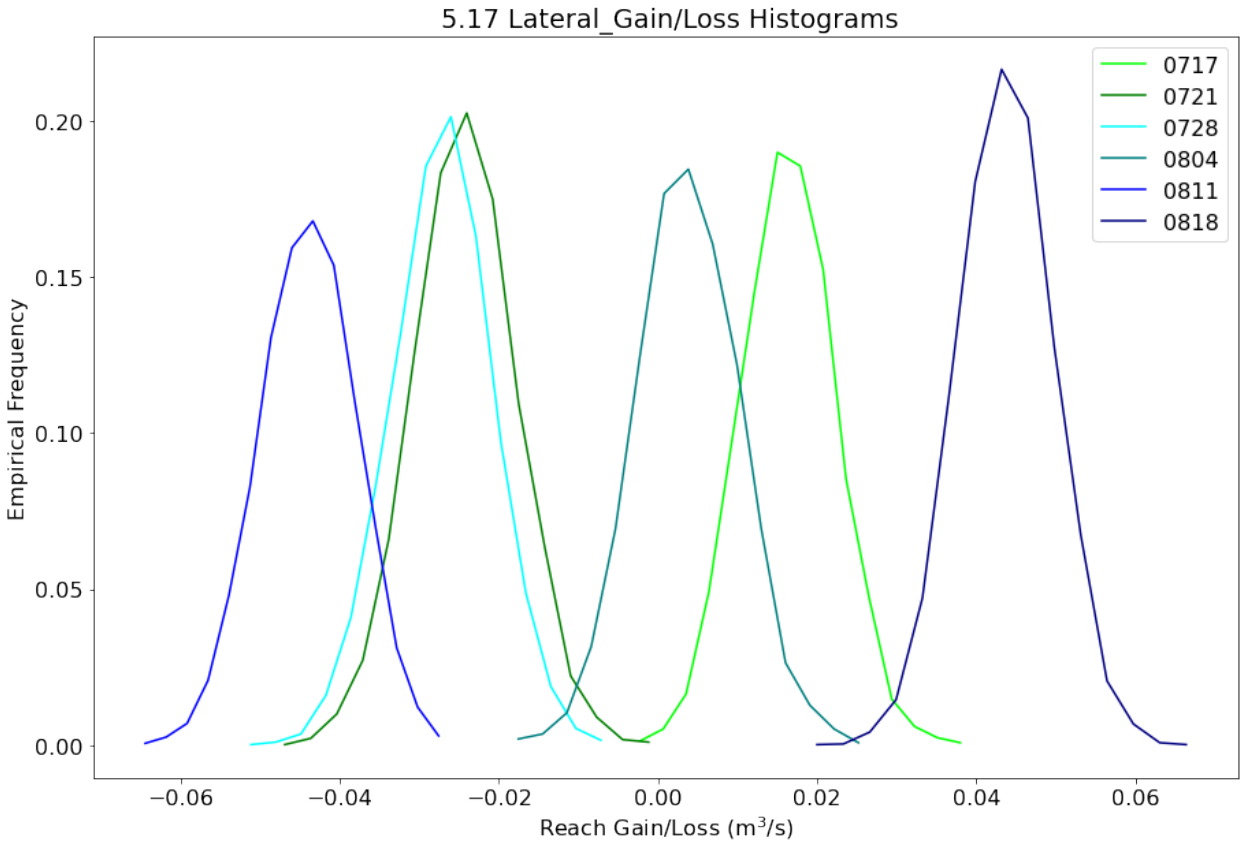


**Figure 2.5 G/L histograms for each sampling date showing variability at 5.17 Lateral**

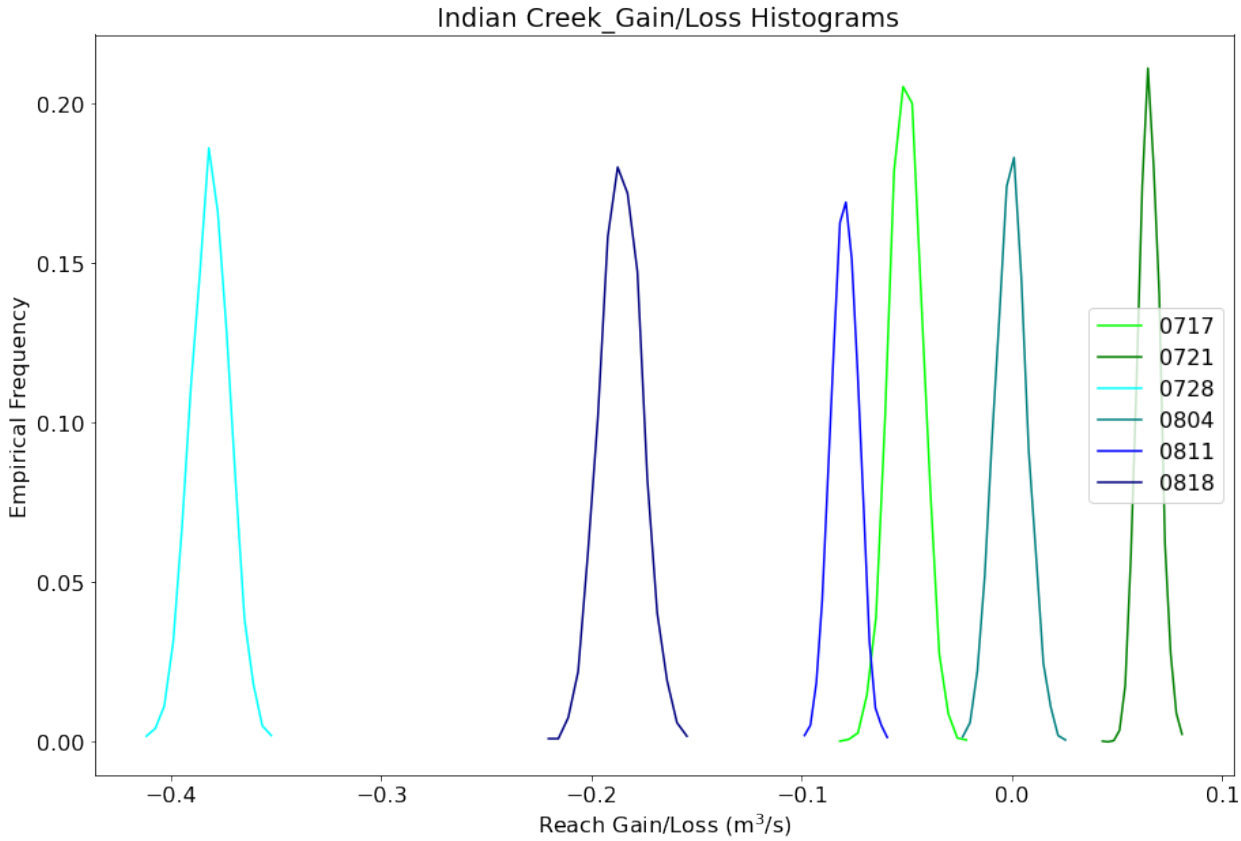


**Figure 2.6 G/L histograms for each sampling date showing variability at Indian Creek**

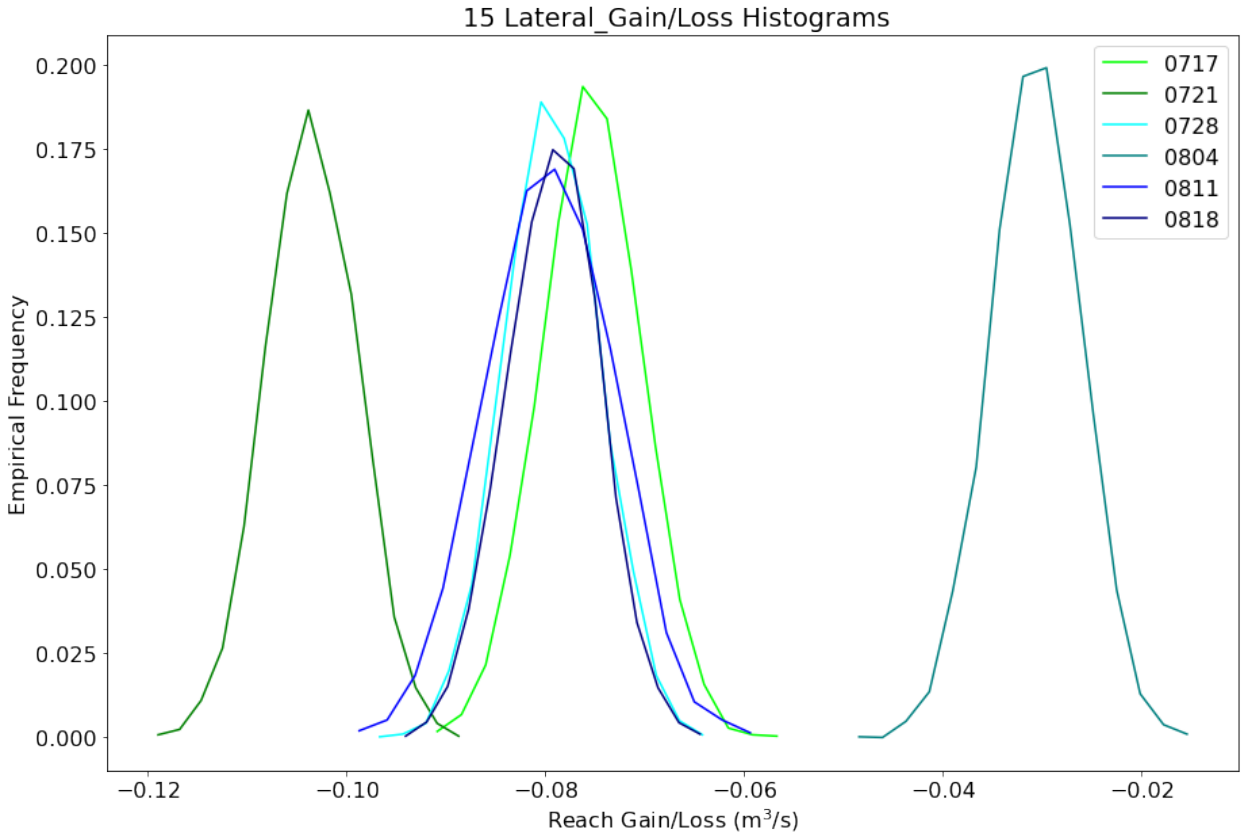


**Figure 2.7 G/L histograms for each sampling date showing variability at 15 Lateral**

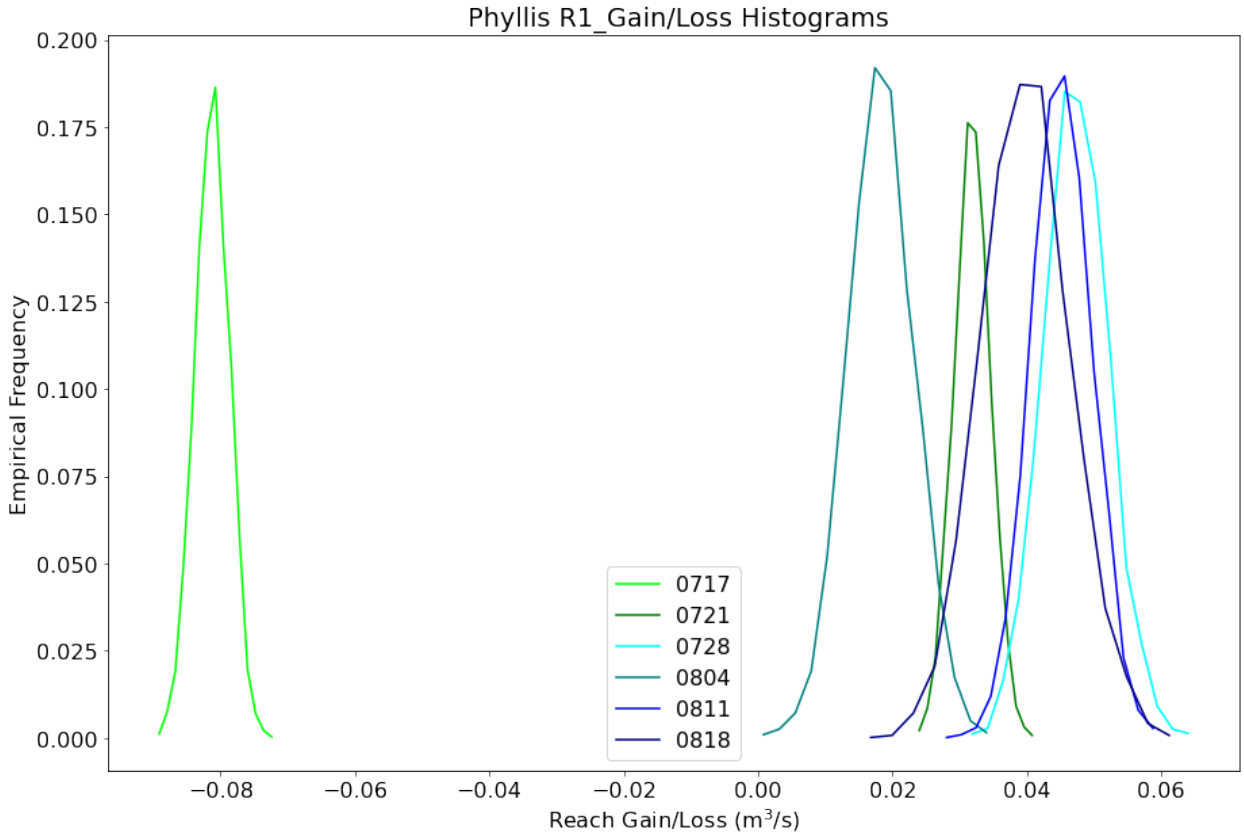


**Figure 2.8 G/L histograms for each sampling date showing variability at Phyllis R1**

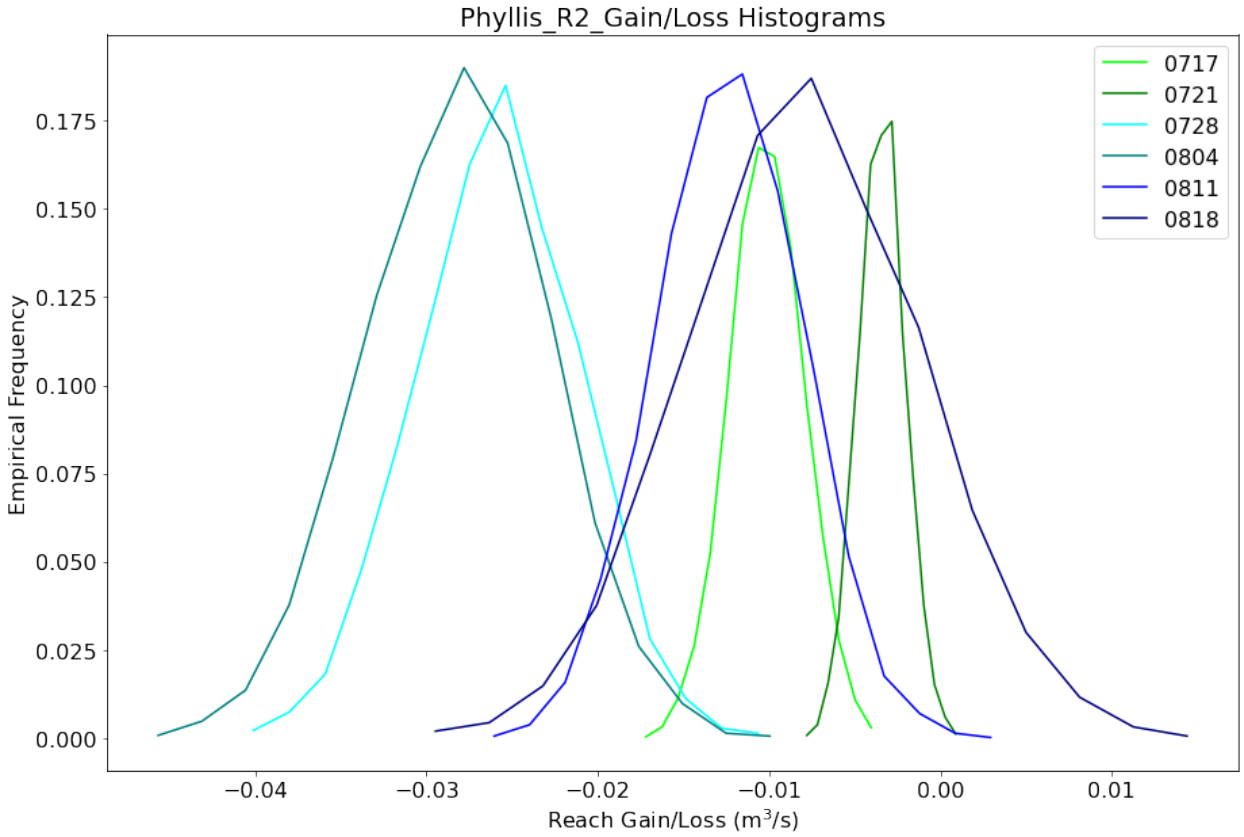


**Figure 2.9 G/L histograms for each sampling date showing variability at Phyllis R2**

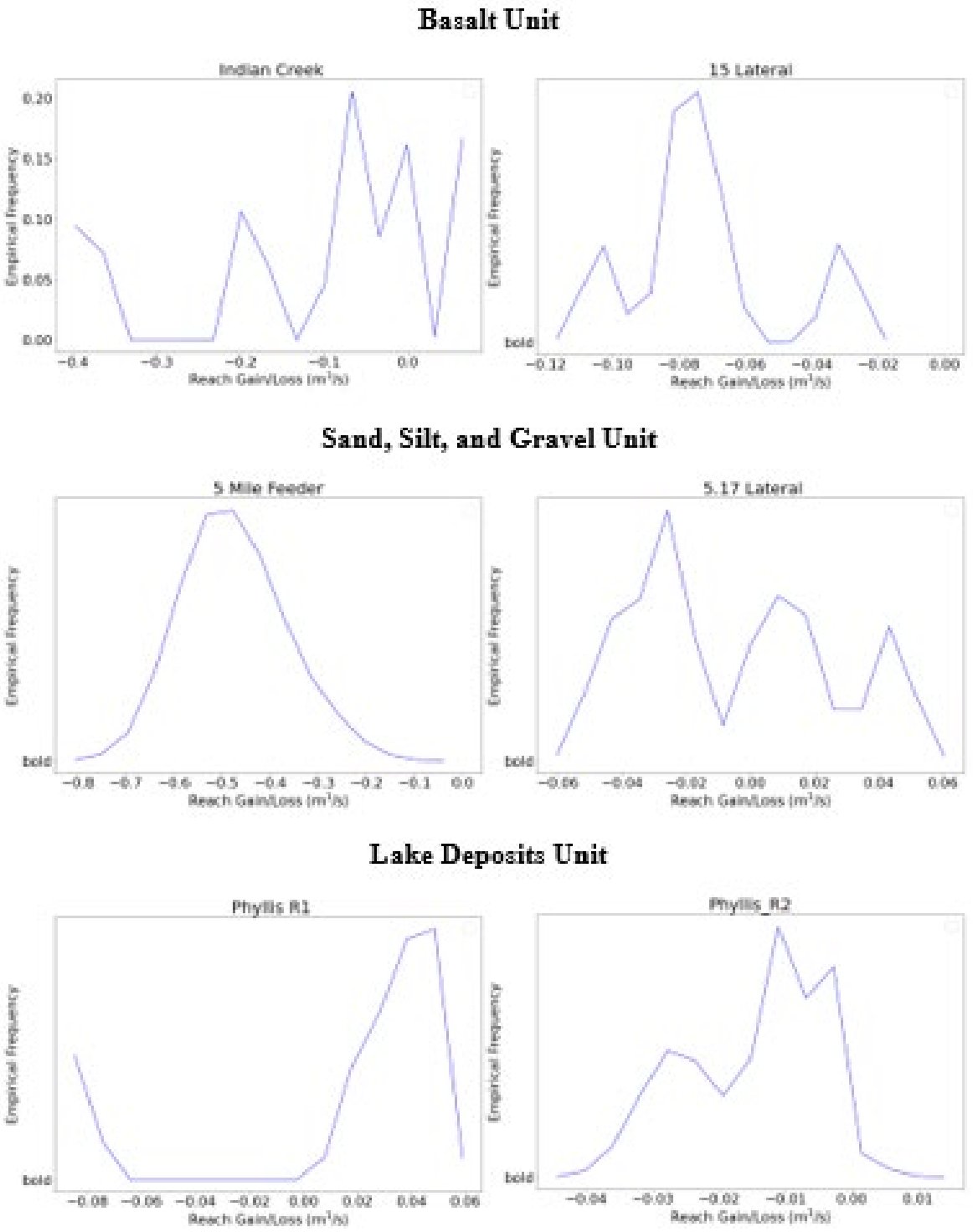


**Figure 2.10 G/L histogram representing all sampling dates for Indian Creek, 15 Lateral, 5 Mile Feeder, 5.17 Lateral, Phyllis R1, and Phyllis R, respectively.**

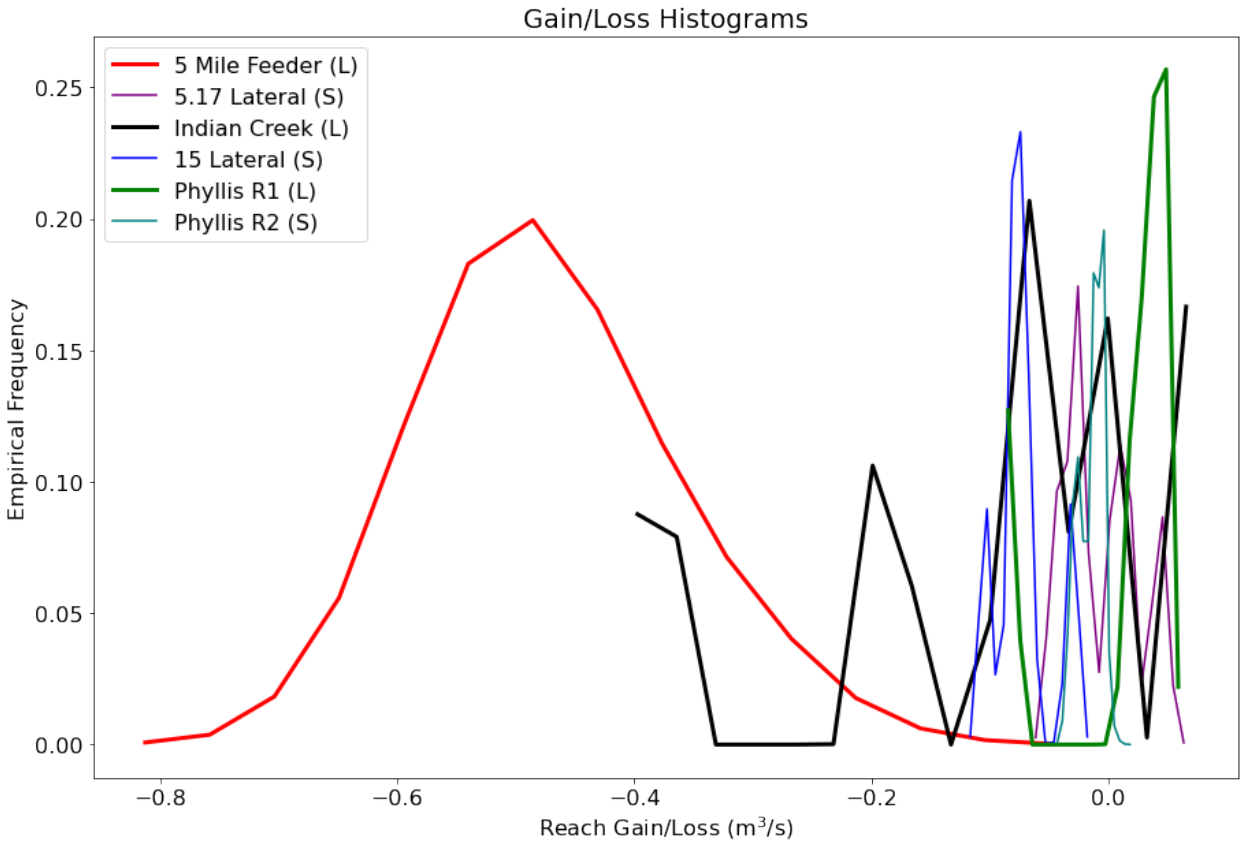


**Figure 2.11 G/L histograms showing variability across lithologic units; 5 Mile Feeder and 5.17 Lateral are located in Gravel, sand, and silt unit, while Indian Creek and 15 Lateral are in Basalt unit, and Phyllis R1 and Phyllis R2 are located in Lake Deposits unit. L and S are large and small, respectively.**

There are statistically significant differences in seepage across canals (Figures 2.10 and 2.11/Table 2.2). For instance, the Fivemile feeder reach (in sand, silt, and gravel unit) loses approximately 0.42 cms on average, while 15 Lateral (in Basalt unit), and Phyllis R2 (in Lake Deposit unit) lose approximately 0.07 cms, and 0.015 cms on average, respectively. The size and lithology affect the magnitude of the seepage rate (Table 2.2). Larger canals passing through the sand, silt, and gravel unit (i.e; Fivemile Feeder) are exchanging more water than reaches in the other lithologic units. The three approaches used for propagating the error in the downstream discharge of the Fivemile feeder showed that the depth variable is substantially affecting the discharge uncertainty more than the

errors in the other parameters as shown in the standard deviations in (Table 1 Appendix A2) where the assumed errors are 10% in A, 1% in B, 0.18 m in depth.

Furthermore, even given measurement errors, the two discharge distributions at the upstream and downstream of a given canal do not overlap and will remain substantially different, implying a high level of confidence in drawing conclusions about their behaviours. The Marsh Mcbirney was sufficient for obtaining information about the gain/loss on canals such as the Fivemile Feeder, implying that another technique is not needed. However, considering the variability of the measurements, the behaviors of 5.17 Lateral, Indian Creek, and Phyllis R1 are uncertain, and we cannot confidently conclude whether they are gaining or losing, and how much water is entering or being lost on average from them. The Indian Creek and 5.17 Lateral, which flow through the TV's two main lithologic units, the Basalt unit and the sand, gravel, and silt unit, increased this uncertainty. As a result, another approach had to be used in these areas in order to learn more about the factors that could be influencing these behaviors.

Three approaches were used to scale the discrete measurements where the resulting net water losses of the TV's canals were 3.23 x 10^6, 1.18 x 10^7, and 1.11 x 10^7 acre ft/yr using Method A', B', and C' respectively. Seepage estimation using the three scaling methods suggest that there is significantly higher seepage across the TV than in previous water budgets of Newton (1991), Urban (2004), Schmidt et al. (2008) and Sukow (2012) (Table 2.3, Figure 2.12). Incorporating canal variability creates significantly different seepage estimates. Method B' shows the highest seepage among the 3 methods. Method C', which includes both size and lithology in seepage calculation, provides an estimate intermediate to Method A' and Method B' (Figure 2.12). Methods A' and B' show

approximately comparable amounts of loss as previous studies in terms of larger canals, but the inclusion of smaller canals changes those values drastically (Figure 2.12). Both Method B` and C` account for lithology in seepage estimation, but including canal size in Method C` caused that most of the seepage is attributed to the larger canals. However, the main contributor to seepage in Method B` is the smaller canals (Figure 2.12) because of their vast spread across the valley. Using these 3 alternative scaling methods, small canals contribute approximately 63% of the total seepage on average.

**Table 2.3 Comparison of canal seepage with previous water budgets**

| Study or Method | | | G/L (acre ft/yr) | G/L (acre ft/yr) *-10^3 |
|---|---|---|---|---|
| Previous water budgets | | Urban (2004), mean of 1996 and 2000 conditions | -573,750 | 574 |
| | | Schmidt et al. (2008) and Sukow (2012), mean 1967–97 conditions | -702,375 | 702 |
| | | Newton (1991), 1980 conditions (Infiltration from surface-water irrigation) | -1,400,000 | 1,400 |
| Current study | The whole TV | Method A` | -3,233,316 | 3,233 |
| | | Method B` "scaled by lithologic unit" | -11,753,372 | 11,753 |
| | | Method C` "scaled by lithology and canal size" | -11,134,458 | 11,134 |
| | Only for 3 Lithologic units | Method A | -2,200,916 | 2,201 |
| | | Method B "scaled by lithologic unit" | -7,187,070 | 7,187 |
| | | Method C "scaled by lithology and canal size" | -6,205,547 | 6,206 |

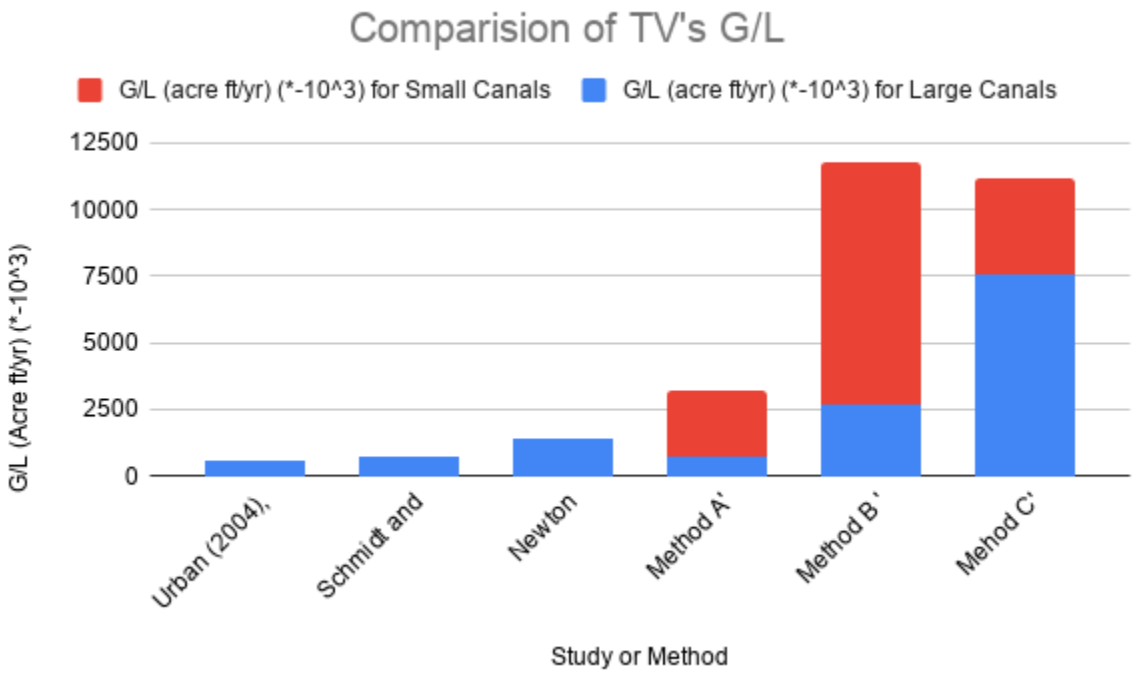


**Figure 2.12 Comparison of TV's seepage quantity with the previous studies**

## 2.4 Discussion

Since seepage from the canal system is the main source of inflows in the TV's water budget (Urban, 2004), accurate estimation of canal seepage is important for better understanding and management of the existing water resources. This is of particular interest in agricultural landscapes such as the Treasure Valley (TV). Several water budgets (Newton, 1991; Urban, 2004; and Schmidt et al., 2008 and Sukow, 2012) estimated the TV's canal seepage, but none of them consider the contribution of the smaller canals or the measurement uncertainties.

We implemented a seepage study on 6 canal reaches of different sizes and underlying lithology in the TV during July and August in the 2020 water year. Our findings

showed that only one canal reach (i.e, Phyllis R1) was gaining (i.e, 0.02 cms) on average, whereas the other reaches were losing water during these July-August seepage runs. Seepage measurements were deployed on 39 irrigation canal and creek reaches in the lower Boise River Basin in June-July and September 1996 where the results showed that the irrigation canals gained and lost water during the June-July seepage runs, whereas most reaches were losing water in September (Berenbrock, 1999). Furthermore, seepage runs were done on three reaches of the lower Boise River in November 1996 to detect the gains and losses of flow after the irrigation season where the two upstream reaches had net gains, while the reach near the confluence with the Snake River, the most downstream, had a net loss. The total gain to the river from the three reaches was 2.57 cubic meter per second (Berenbrock, 1999).

There is a significant seepage variability across the TV. This seepage variability is attributed to lithologic unis and canal size variation. This seepage variability has implications for water resources management by supporting the types of management strategies that should be implemented. For instance, in a location that has considerable losses such as Fivemile Feeder, a manager could line the canal to increase surface water availability to irrigators, while if the manager wanted to increase the GW aquifer recharge, this location might be useful for replenishing the aquifer. Moreover, the gain/loss method using the Marsh Mcbirney in this study was sufficient for specific canal reaches such as the Fivemile Feeder to obtain information on their gain/loss. However, the gain/loss of Indian Creek and 5.17 Lateral, which flow through the TV's two main lithologic units (the Basalt unit and the sand, gravel, and silt unit) is uncertain, which requires applying another approach in these two lithologic units to investigate the controlling factors of this

uncertainty. We believe that the key reason controlling the gain/loss uncertainty in 5.17 Lateral is that this reach is perpendicular to a large reach of the Phyllis canal which may cause side flows between the two reaches based on the local hydraulic gradient. Furthermore,

Seepage was estimated across the TV using three alternative scaling approaches; these estimates showed that seepage across the TV is significantly higher than in previous studies (Newton, 1991; Urban, 2004; Schmidt et al., 2008 and Sukow, 2012) (Figure 2.12/Table 2.3). This was anticipated because those previous water budgets did not include the vast network of small canals or account for canal seepage variability and uncertainty. However, the estimates made in this study may have additional unquantified uncertainty given the different assumptions we made for each process. Method A` was the most simple approach, where canal properties were not taken into account, but these characteristics were incorporated in methods B` and C`. It is clear from the differences between the total seepage estimate between Method A` and Methods B` and C` that incorporation of variability in canal characteristics can create significantly different seepage estimates. Although Methods A` and B` seem to have seepage amounts approximately similar to previous studies from larger canals, including the smaller canals significantly changes those estimates (Figure 2.12). Most of the seepage estimate using Method B` is attributed to the smaller canals, which represent the majority of the canal system of the TV. We found that the total TV seepage is significantly variable based on the method implemented to scale those measurements. Uncertainty of estimated seepage using methods B` and C` is expected to be high because of the assumption that two canal reaches reflect each lithologic

unit and that one of them represents a particular scale, despite the fact that measurements vary significantly across the valley. To address this seepage variability, we recommend doing additional measurements to better capture the canal variability and decrease the uncertainty related to these methods. Two measurements might not be sufficient for each unit, and we believe that additional measurements are necessary to capture additional sources of canal variability within each unit. For example, within each lithological unit it may be necessary to account for variability in canal material and condition (e.g., unlined vs. lined, degree of vegetation growth, etc.) and size. To capture this variability and mitigate the uncertainty of the total seepage magnitude across the TV using the 3 scaling methods, we need at least the actual width of the canals rather than having only the general description as small versus large, and the canal structure and whether it is lined or not. Since we have a significant number of various factors and properties affecting the seepage magnitude, which cannot be examined totally, we recommend using statistical methods such as fixed and mixed effects models for determining the marginal value of additional observations. Such models use mathematical models to describe how the dependent variable (i.e; canal seepage) is some function of one or more independent variables (i.e, canal size, lithology, structure, lining, and seasonality) while assuming that these independent variables are fixed. If the independent variables are drawn at random from a large population of canals to have a sample representative of the wider population of models that exist, then the models represent random effects. If the main purpose is to test the effect of a factor or a covariate on the dependent variable (i.e; seepage), then we should use the fixed effect model. However, if we are sampling factor levels from a larger population, our choices are likely random (we select the factor level that we are particularly

interested in. To avoid neglecting a lot of data and improve the seepage estimate, a better alternative model is to model a random effect properly in our analysis by using the powerful mixed effects models which allow a mixture of fixed and random effects. For instance, Akbar et al. (2018) developed a predictive model based on electromagnetic inductance (EM31) imaging techniques and data from direct measurements of channel seepage, where the main output was seepage values through the channels. They used three modelling methods; Generalised Linear Mixed (GLM) model, Random Forest (RF) model and Generalized Boosted Regression Model (GBM), where the RF model showed the best performance to locate channel seepage hotspots and determine the magnitude of their losses. Instead of doing flow measurement across the whole canal system of different sizes and structures and passing through various lithologic units, these models might be good to design the campaign to characterize those canals while balancing the additional cost because there is no need to have measurements everywhere in this system.

Using the 3D velocimeter Acoustic Doppler current profiler (ADCP) might be valuable to get additional flow measurements with more precise error, but We favored deploying the Direct Current (DC) Resistivity on one position in the Basalt unit as a starting point to obtain the flow path pattern and a more detailed picture of the regulating subsurface conditions over using the ADCP. This method will be presented in detail in Chapter 3.

## References

Akbar, M., & Irohara, T. (2018). Scheduling for sustainable manufacturing: A review. *Journal of cleaner production*, *205*, 866-883.Berenbrock, C. (1999). Streamflow Gains and Losses in the Lower Boise River Basin, Idaho, 1996-97. Water-Resources Investigations Report, 99, 4105.

Boning, C. W. (1992). Policy statement on stage accuracy. Technical Memorandum No. 93-07. Washington, D.C.: USGS, Office of Water.

Cheremisinoff, N. P. (1998). Groundwater remediation and treatment technologies. Elsevier.

Harmel, R. D., Cooper, R. J., Slade, R. M., Haney, R. L., & Arnold, J. G. (2006). Cumulative uncertainty in measured streamflow and water quality data for small watersheds. Transactions of the ASABE, 49(3), 689-701.

Idaho Department of Water Resources, (1997). Map and GIS database: Boise Valley Project, Land Use and Land Cover, 1994. Based on 1:12,000 scale CIR photography. Map scale: 1:100,000.

Kjelstrom, L.C. (1995). Streamflow gains and losses in the Snake River and ground-water budgets for the Snake River Plain, Idaho and eastern Oregon: U.S. Geological Survey Professional Paper 1408-C, p. C1-C47; 1 plate in pocket.

Lewis, R.S., Link, P.K., Stanford, L.R., & Long, S.P. (2012). Geologic map of Idaho: Moscow, Idaho Geological Survey M-9, scale 1:750,000, 1 sheet, 18 p. Booklet.

Newton, G.D. (1991). Geohydrology of the regional aquifer system, western Snake River plain, southwestern Idaho: U.S. Geological Survey Professional Paper 1408-G, 52 p., 1 plate in pocket.

Pelletier, P. M. (1988). Uncertainties in the single determination of river discharge: A literature review. Canadian J. Civil Eng. 15(5): 834-850.

Petrich, C.R. (2004b). Treasure Valley Hydrologic Project executive summary: Moscow, University of Idaho Water Resources Research Institute, Research Report IWRRI-2004-04, 33 p.

Sauer, V. B., & R. W. Meyer. (1992). Determination of error in individual discharge measurements. USGS Open File Report 92-144. Washington, D.C.: USGS.

Schmidt, R.D., Cook, Z., Dyke, D., Goyal, S., McGown, M., & Tarbet, K. (2008). Distributed parameter water budget data base for the lower Boise Valley—U.S. Bureau of Reclamation. Pacific Northwest Region, 109 p.

Slade, F. M., Jr., Bentley, J. T., & Michaud, D. (2002). Results of streamflow gain-loss studies in Texas, with emphasis on gains from and losses to major and minor aquifers: U.S. Geological Survey Open-File Report 02-068, published on CD-ROM.

Sukow, J. (2012). Expansion of Treasure Valley Hydrologic Project groundwater model: Boise, Idaho Department of Water Resources, 34 p.

Urban, S.M. (2004). Water budget for the Treasure Valley aquifer system for the years 1996 and 2000: Moscow, University of Idaho Water Resources Research Institute, Research Report unnumbered, variously paged.

# CHAPTER 3: CHARACTERIZING CHANNEL LOSSES USING DIRECT CURRENT RESISTIVITY

## 3.1 Introduction

Geophysical methods are increasingly used to complement traditional hydrogeological measurements. For example, methods like determination of hydraulic head , the direction of local groundwater flow, and estimating hydraulic conductivity can be complemented and, in some cases, completely replaced by geophysical methods (Attwa and Günther, 2012). Direct Current (DC) resistivity is an electrical geophysical survey used for making measurements on the ground surface to get the subsurface resistivity distribution which in turn can be used to calculate the subsurface true resistivity. The resistivity value we measure in the field is not the true resistivity, but an "apparent" value for the subsurface. Both apparent and true resistivities are equal if the subsurface is uniform, but in reality, the subsurface is heterogeneous and the apparent resistivity has a value between the maximum and minimum true resistivities. This resistivity distribution is a reflection of several geological parameters such as mineral and fluid content, porosity, and degree of water saturation in the rock. DC has been used in many aspects such as groundwater exploration (Gautam and Biswas, 2016; Oyeyemi et al., 2018a, b), engineering investigations (Oladunjoye et al., 2017; Oyeyemi et al., 2017, 2020), and environmental studies (Rosales et al., 2012; Akinola et al., 2018; Olaojo et al., 2018; Olaseeni et al., 2018; Attwa et al., 2021). Attwa et al. (2021) integrated between the DC, GIS, and Remote Sensing for sustainable water resources management in structurally-

controlled watersheds in arid environments; they located potential areas suitable for surface water harvesting into subsided blocks within the impermeable crystalline rocks.

The two-dimensional 2D resistivity surveys are more accurate than the 1D resistivity soundings because they account for the resistivity changes in both vertical and horizontal directions along the survey line (Loke, 2004). 2D Electrical Resistivity Imaging (ERI) is a well-established method for subsurface hydrogeological investigations at lab and field scales such as infiltration rate estimation (Hübner et al., 2017), potential aquifer zones' delineation, contaminant flow detection, and imaging of wastewater and oil leakages in soils (Attwa and Zamzam, 2020; Moreira et al., 2020). In the current seepage study, we aim to use 2D ERI as a complementary method to be integrated with the gain/loss method to provide additional insight into GW-SW interactions in the TV. This chapter includes two applications of DC resistivity methods, a hydrogeophysical simulation using COMSOL Multiphysics and DC resistivity measurements from a real-world canal site.

Using a model to simulate an outcome is known as forward modeling where the forward problem is to get the model to generate data from an input or a problem of estimating what should be observed for a specific model such as calculating the resistivity variation that would be observed for a given model of a canal seeping in a specific lithologic unit. Forward model takes a set of parameters and generates data that can be compared to observational data. This forward modeling is needed in the electrical prospecting method to detect the distribution of the potential subsurface anomalies and structures (Wang et al., 2011; Butler and Sinha, 2012; Song et al., 2017; Udosen and George, 2018; Gao et al., 2020). One advantage of forward modeling is that it allows adjusting the model parameters to fit observations (Sanuade et al., 202). Forward modeling

is necessary in any inversion algorithms (Gao et al., 2020). The main objective of the inversion process is to find a subsurface model whose response is in agreement with the actual measured values subject to certain restrictions. This model is an idealized mathematical representation of one of the earth sections (Loke, 2004). It has a set of parameters or physical quantities that needs to be estimated based on the observed data. The model response is the synthetic data calculated from the mathematical relationships defining the model for a given set of model parameters. The finite-difference (FD) (Dey and Morrison, 1979a, 1979b) or finite-element (FE) (Silvester and Ferrari, 1990) methods provide the mathematical relation between the model parameters and its response for the 2-D and 3-D resistivity models. FD or FE algorithms are used to determine the direct current response of the current model section as well as the sensitivity of measured data to correct the model parameters. The resistivity distribution is approximated in both methods by a mesh of individual elements or cells, each with constant resistivity. The potential is then computed at discrete points (mesh nodes) by solving a linear system of equations derived from a discretized differential equation and boundary conditions (Binley and Kemna, 2005).

## 3.2 Methods

### 3.2.1 Synthetic / Forward Modelling Using Comsol Multiphysics

Hydrogeophysical simulation is a process to synthesize predicted distributions of electrical resistivity given potential configurations of sensor arrays and alternative hypotheses of subsurface conditions (such as porosity, hydraulic conductivity, and variability in soil water content). This simulation will provide a preliminary basis for examining how hydrogeophysics may be useful for monitoring surface water-groundwater

interactions in managed water resource systems and refine the design of potential future field investigations in terms of the distribution and density of the sensor array. To do this simulation, COMSOL Multiphysics was used as a powerful tool for numerical computation; forward calculations are simple and more informative using COMSOL because features in the post-processing stage can be visualized (Sanuade et al., 2021). In addition, Comsol Multiphysics is widely used in Electrical Resistivity Tomography (ERT) which is a method based on the study of the capacity of the subsurface to resist an electrical current. Sanuade et al. (2021) tested COMSOL Multiphysics' efficiency for numerical modeling and subsurface electrical potentials simulations by comparing its numerical modeling output with the calculated analytical solution. Their study demonstrated that both solutions were in agreement which proved COMSOL effectiveness and reliability in investigating the DC resistivity method forward modeling. So, COMSOL Multiphysics was used to simulate the distribution of electrical potentials of point source in 3D space which in turn was converted to an apparent resistivity distribution that would be expected given a canal water flow model in different lithologic units.

The potential distributions that would be expected given subsurface structures can be determined by forward modeling. The resulting apparent resistivity values are in turn used to determine the true subsurface resistivity image using the inversion process; inverting the electric potential data measured in the field, and forward modeling as an important step for any inversion algorithms (Gao et al., 2020).

Forward modelling is essential for implementing the resistivity data inversion to obtain the true resistivity of the subsurface layers. However, the main objective of the simulation in this project was to create a number of endmembers representing different

resistivity distributions that might be expected given specific assumptions. We applied this simulation through two different lithologic units; basalt unit and sand, gravel and silt unit. These two lithologic units are the largest ones covering the TV and the gain/ loss uncertainty quantification is significantly high in these two units especially through the Indian Creek reach which is representing the wider reach passing through the Basalt unit. In this study, forward modeling of direct current (DC) resistivity was applied to get a preliminary basis of the expected resistivity variation that would occur as a result of potential seepage from the adjacent canal given the assumptions that the subsurface system consists of a simple single lithology (i.e; subsurface is assumed to be either sand, gravel and silt unit, or basalt unit with no vertical or lateral variation). This simulation was applied while there is no water in the adjacent canal and during the irrigation season separately. Any lateral or vertical change in the subsurface resistivity would result in a change in the apparent resistivity (ρa) (Telford et al., 1990). Since the time between the dry and irrigation seasons is not long, the expected change in the subsurface resistivity distribution would be attributed to the variation in the water content in the rocks. We coupled water flow and electric current flow using two modules in the finite-element-COMSOL multiphysics software (COMSOL Multiphysics Users' Guide, 2017). These two modules are AC/DC conductive-media module and porous media and subsurface flow module.

Generally, there are three sections in COMSOL Multiphysics; 1) pre-processing, which involves finite-element model and setting the parameters, 2) solution, which involves generating the mesh and solving equations, and 3) post-processing for visualizing and analyzing the results (COMSOL Multiphysics Users' Guide, 2017). For the plane geometry setup in the preprocess, a 3D trapezoid canal with the dimensions (6 m and 2 m

wide at the top surface and the bottom, respectively, and 4 m deep) was created in a domain with X, Y, and Z of 500, 100, 50 m dimensions, respectively as shown in figure (3.1). The physics interfaces used in this study were Richards' equation and electric currents. The subsurface flow module has different interfaces that account for different flow characteristics. Richards' equation physics interface was chosen for this study because it is more appropriate for describing nonlinear flow in variably saturated porous media to analyze unsaturated zone processes. Richard's equation is a two-phase (e.g; water and air) porous media interface describing slow water movement in a partially saturated media where relative permeability changes with fluids' movement through the porous matrix.

$$\rho((Cm/\rho\, g) + SeS) + \partial p/\partial t + \nabla \cdot \rho(-\kappa s/\mu * kr\,(\nabla p + \rho\, g\, \nabla D)) = Qm \quad (3.1)$$

where p (pressure) is the dependent variable. Cm denotes the specific moisture capacity, Se is the effective saturation, S is the storage coefficient, κs denotes the hydraulic permeability, μ is the fluid dynamic viscosity, kr represents the relative permeability, ρ is the fluid density, g represents gravity acceleration, D is the elevation, and Qm is the fluid source (positive) or sink (negative).

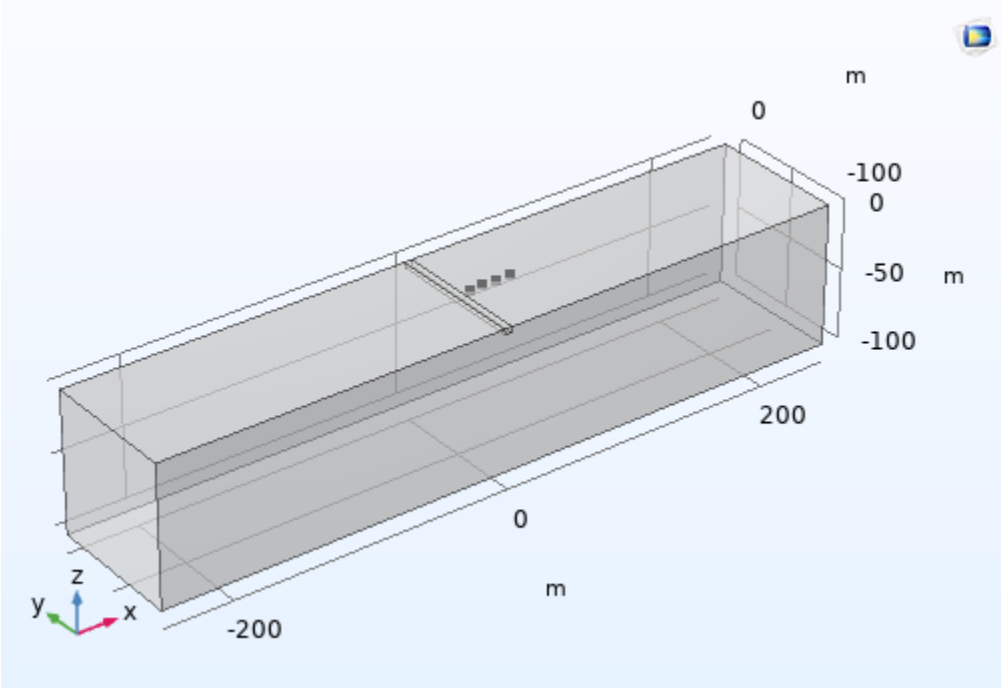


**Figure 3.1 3D model geometry**

COMSOL Multiphysics solves Richards' equation for a pressure dependant variable (e.g; Figure 3.2) in the same way as Darcy's law does, but it also has options for setting the hydraulic head or pressure head values on the model's boundaries, either directly or as part of the Pervious Layer boundary condition. Moreover, make use of the hydraulic and pressure heads during the evaluation of the results (Subsurface Flow Module Users' Guide, 2018).

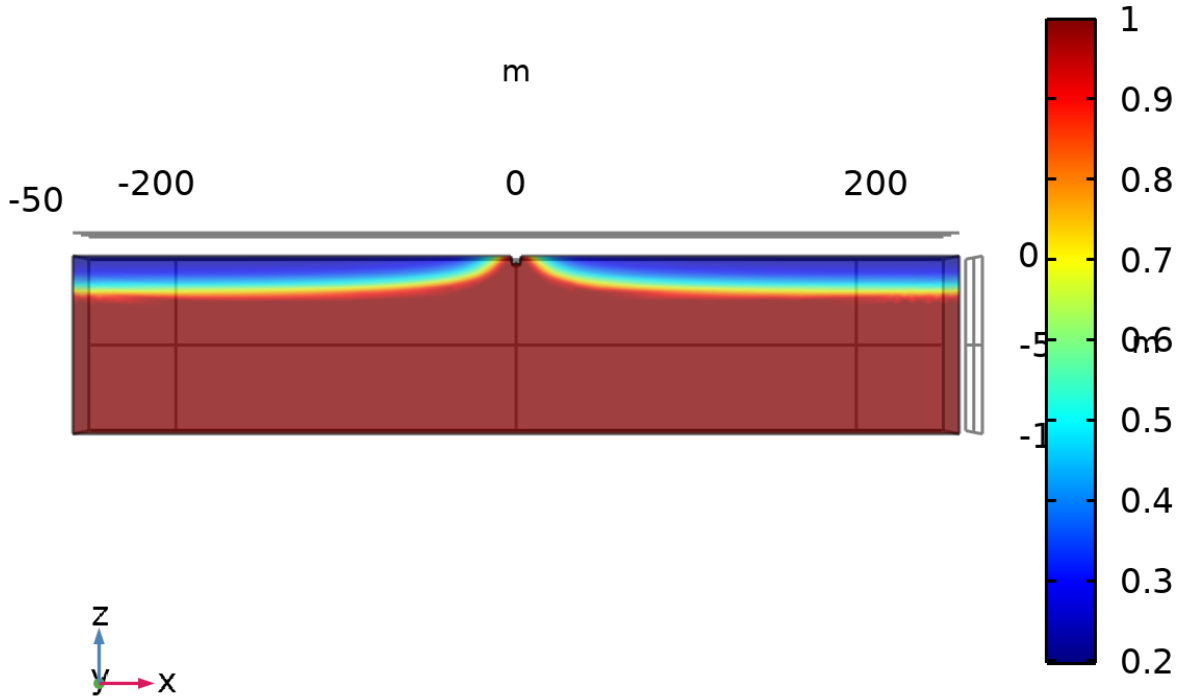


**Figure 3.2 Example for distribution of the dependant variable (pressure) solved by Richards' equation in COMSOL Multiphysics**

Richard's equation is a highly non-linear coupling because permeability changes significantly depending on what proportion air to water is. For Richards' equation interface, air is assumed to be at the atmospheric pressure, Darcy's velocity is only for the wetting phase, and the Van-Genuchten retention curve was used.

Assumptions and Parameterizations:

The study was assumed to be in a steady state with parameters changed based on which lithologic unit and surrounding conditions were chosen. To make this simulation computationally simple, the average of the effective material properties such as porosity and permeability were used (i.e; the domain was homogenized by avoiding the need to mesh complex geometries) to solve for the flow pressure and velocity. Regarding the boundary conditions, the water table was assumed to be at 25 m, and 10m below ground surface in the Sand, Silt, and Gravel unit, and Basalt unit, respectively. Depth to water in

the canal (in the irrigation season) is assumed to be at 1 m below ground surface (i.e; water depth in the canal is 3 m). We assumed that the mesh structure is coarse for the Basalt unit and finer for the Sand, Silt, and Gravel unit. The saturated soil water content (Θs), and residual soil water content are assumed to be 0.3, and 0.01 for Sand, Silt, and Gravel, respectively and 0.2 and 0.068 respectively for the Basalt unit because basalt matrix is considered as silt/clay-like nature. Effective saturated hydraulic conductivity (Ks) is assumed to be 5 x 10^-6 m/s for Sand, Silt, and Gravel unit and 3.53 x 10^-4 m/s for the Basalt unit (i.e; 30.5 m/day for permeable basalt). The Van-Genuchten water retention parameters ($\boldsymbol{\alpha}$, and n) were assumed to be 0.2 1/m and 2, respectively for Sand, Silt, and Gravel unit, while 0.49 1/m and 3 for the Basalt unit. Cementation factor was 2 for both units, while the saturation exponent was 3 for the Basalt, and 2 for the Sand, Silt, and Gravel unit.

Modeling Design

Four evenly spaced points, representing 2 current electrodes for injecting current through the subsurface and 2 potential electrodes for measuring the voltage difference between the 2 potential electrodes at each measurement point, were located beside the canal where the closest electrode was 2 meters away from the canal (Figure 3.1). The electrodes arrangement follows the Wenner alpha array. The number of electrodes, total line length, minimum and maximum electrode spacing are 143, 142 m, 2 and 46 m, respectively to get 828 total number of datum points of 23 data levels and a total investigation depth of 23 m below ground surface. The minimum and maximum electrode coordinates are 5 and 147m, respectively beside the suggested canal. An electric current (I) of 1 A was injected after the survey line setup at the top of the block into the subsurface through the point source.

3.2.2 Field DC Resistivity Data Collection

3.2.2.1 Background

The electric current flows through the ground based on the physical Ohm's Law which is fundamental in resistivity surveys. Ohm's Law (in vector form) for current flowing in a continuous medium is given by:

$$J = \sigma E \qquad (3.2)$$

Where **σ** is the medium conductivity, J is the current density and E is the electric field intensity. The electric field potential is what we measure in reality, while the medium resistivity (**ρ**) (the reciprocal of the conductivity (**ρ**=1/**σ**)) is more commonly used. The relationship between the electric potential and the field intensity is given by:

$$E = -\Delta\Phi \qquad (3.3)$$

$$E = -\sigma\Delta\Phi \qquad (3.4)$$

When a point current source on the ground surface injects current into the ground, the electrical potential in the ground is determined by:

$$\Delta\Phi = \frac{\rho I}{2\pi r} \qquad (3.5)$$

Where r is the distance of the location from the current electrode. A pair of current electrodes (positive and negative) are usually used in resistivity surveys where the potential distribution in the medium from such a pair is given by equation (3.6), and if two potential electrodes are used, the measured potential difference is given by equation (3.7)

$$\Delta\Phi = \frac{\rho I}{2\pi r * \left(\left(\frac{1}{rc_1}\right) - \left(\frac{1}{rc_2}\right)\right)} \qquad (3.6)$$

$$\Delta\Phi = \frac{\square\square}{2\square\square * \left(\left(\frac{1}{\square\square_1\square_1}\right) - \left(\frac{1}{\square\square_2\square_1}\right) - \left(\frac{1}{\square\square_1\square_2}\right) + \left(\frac{1}{\square\square_2\square_2}\right)\right)} \qquad (3.7)$$

Equation 3.6 gives the measured potential over a homogeneous half space of a 4 electrodes array. However, the field surveys are carried out over an inhomogeneous medium with a 3-D distribution of subsurface resistivity. Resistivity measurements are made by measuring the potential difference at two potential electrodes (P1 and P2) resulting from a current injected through two current electrodes (C1 and C2) into the ground. Apparent resistivity (pa) values are given by current (I) and potential ($\Delta\phi$) values

$$\rho a = K\frac{\Delta\Phi}{I} \qquad (3.8)$$

Where **ρ**a is the apparent resistivity which practically can be calculated using equation (3.9) because resistivity instruments usually measure resistance values ($R = \Delta\phi/I$), and K is the geometric factor which depends on the arrangement of the four electrodes.

$$\rho a = KR \qquad (3.9)$$

$$K = \frac{2\pi}{\left(\left(\frac{1}{rc_1p_1}\right) - \left(\frac{1}{rc_2p_1}\right) - \left(\frac{1}{rc_1p_2}\right) + \left(\frac{1}{rc_2p_2}\right)\right)} \qquad (3.10)$$

3.2.2.1 Site Selection

Based on findings from Chapter 2, there was significant uncertainty in gain/loss quantification in canals passing through the Basalt unit (i.e; Indian Creek) and Sand, Silt, and Gravel unit (in 5.17 Lateral). So, Indian Creek and 5.17 Lateral were the best locations

to apply the DC resistivity method for two reasons; they flow through the Basalt unit and Sand, Silt, and Gravel unit which cover more than 30% and 19%, respectively of the TV's total area, and gain/loss through them is uncertain. However, doing the resistivity measurements in these locations has been denied by the owners of the lands adjacent to these canals. We have identified an alternative site for the geophysical measurements in the Basalt unit where a Phyllis canal of size similar to Indian Creek is passing through it. This site is located at 43°35'17.5"N 116°35'01.7" W at Lions Park (Figure 3.3), where we have received permission from the City of Nampa, Idaho. The rebars were conducted to deploy the DC measurements twice; in March and April before and after the irrigation season started.


**Figure 3.3 DC profile location map**

3.2.2.2 Data Acquisition

A two-dimensional electrical tomography survey line was carried out using 72 electrodes of 2m- spacing connected to a multi-core cable where this survey line was straight and perpendicular to the side of Phyllis canal and the first electrode is 1 m away from the edge of the canal (Photo 3.1). The sequence of measurements, array type and other survey parameters were prepared and uploaded to the Syscal Pro 72 before the field work. Each array has specific characteristics such as investigation depth, the array sensitivity to vertical and horizontal changes in the subsurface resistivity, horizontal data coverage, and its signal strength (Loke, 2004). Among the most commonly used arrays for 2-D imaging (Wenner, dipole-dipole, Wenner- Schlumberger, pole-pole, and pole-dipole), Wenner Alpha was selected for this survey because it has the strongest signal strength (Loke, 2004) which is an important factor since the survey was carried in the Basalt system which was expected to cause significant background noise. The geometric factor used to measure the array's apparent resistivity value is inversely proportional to signal strength; the geometric factor for the Wenner array is 2a which is smaller than the others of other arrays (Loke, 2004). After system setup, a resistivity check was performed to detect if there is any systematic noise to fix it before starting the survey. This noise usually occurs during the survey where breaks in the cable, very weak ground contact at an electrode so that adequate current cannot be applied into the ground, failing to attach the clip to the electrode, or attaching the cables in the wrong direction are all possible causes of this noise (Loke, 2004). Syscal Pro 72 was used to collect Electrical Resistivity Imaging (ERI) data twice; the first one was measured on March 8th, 2021 before the irrigation season starts, and the second profile was collected on April 26th after the irrigation season started on April 1st,

2021 to monitor the flow pattern, the temporal changes of the rock saturation, and how the canal seepage influence the local groundwater aquifer to better understand this heavily managed system. The profile length was 142 m using 72 point electrodes with 2 m of spacing between. The first step of data acquisition was done by recording all the possible measurements with Wenner Alpha array of an electrode spacing of "1a" (i.e; 2 m), then repeating the same procedure for "2a", "3a",.. ,etc, until "23a" resulting in 828 data points and a median depth of investigation of approximately 23 m (0.5*a). The contact resistance values were better in the second survey because the surface layer was wet due to the rainfall that occurred on April 26th. This 2D profile survey line, fixed over the time-lapse ERI measurements period (March-April) to monitor the resistivity change over time, is shown in a location map (Figure 3.3, Photo 3.2). During the survey, the measured apparent resistivity data were stacked to improve the data quality (i.e., stacking error ~<3%).

**Photo 3.1 First electrode installed at approximately 1 m away from the canal edge**

**Photo 3.2 2D ERT Data acquisition in Lions Park, Nampa**

#### 3.2.2.2 2D Forward Modelling and Inversion

In this study, the Direct Current 2D Inversion and Resolution (DC2DInvRes) was used for data analysis (Günther, 2007). It is a Finite Difference Forward Operator. The 2D processing involved data filtering by eliminating poor quality data-points that display abrupt shifts over the measured points (Figures 3.4- 3.5); only 5 points were eliminated representing <1% of the total 828 measured data points. Smoothness constraints and the Gauss–Newton inversion algorithm were used to regularize the data. The 2D finite difference (FD) technique which is based on the construction of a discrete model in form of a hexahedral grid with nodes at the cell corners (Günther, 2004), was used to solve the forward calculations of 2D-ERI. We used fixed regularization ($\lambda = 80$ and z-weight = 0.3) and first-order smoothness constraints; the inversion parameters (LAMBDA, and ZWEIGHT) were selected to ensure that the inversion algorithm could capture the subsurface horizontal and vertical variations (Audenrieth et al., 2020). An advanced inversion scheme was applied to produce a reliable interpretation (Clément et al., 2010, and El-Saadawy et al., 2020). The least-squares optimization method was used where an initial model was iteratively improved to minimize the difference between the model response and the observed data (i.e,.Root Mean Square Error (RMSE) gets closer to zero). The scatter plot (Figure 3.6) shows the fitting between the measured resistivity of electrode configuration and the resistivity calculated in the forward modelling step (i.e; what you actually measured and what you would expect). This plot shows that the measured and calculated apparent resistivities line nicely on a diagonal which shows that they are very close to each other.

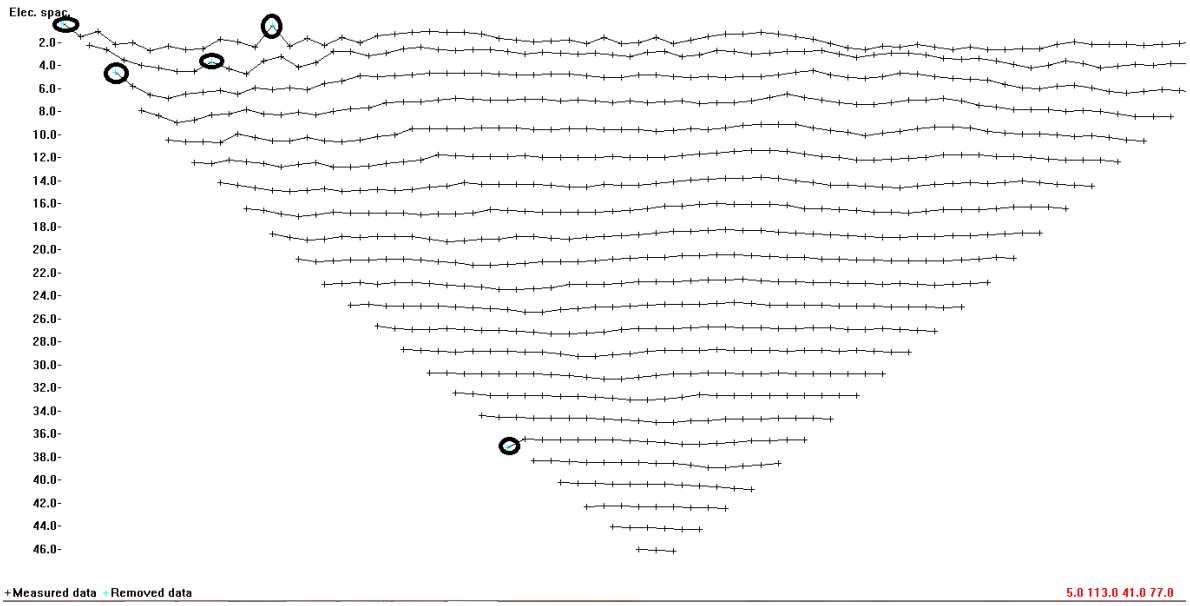


**Figure 3.4 Data filtering by rejecting bad quality data-points from the 1st set of measurements**

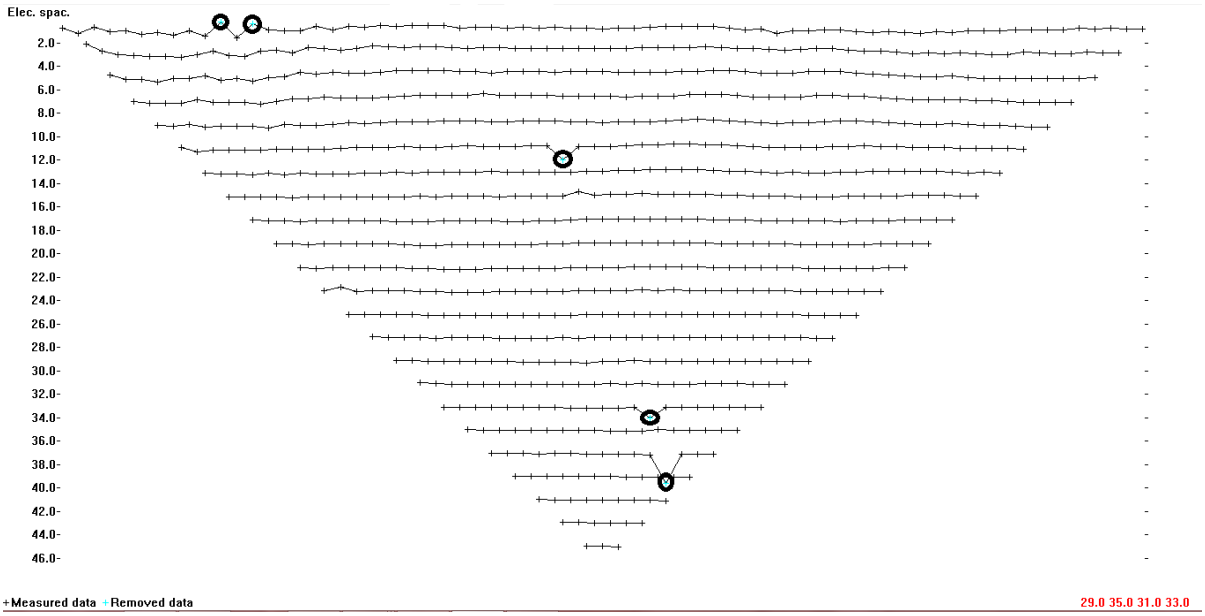


**Figure 3.5 Data filtering by rejecting bad quality data-points from the 2nd set of measurements**

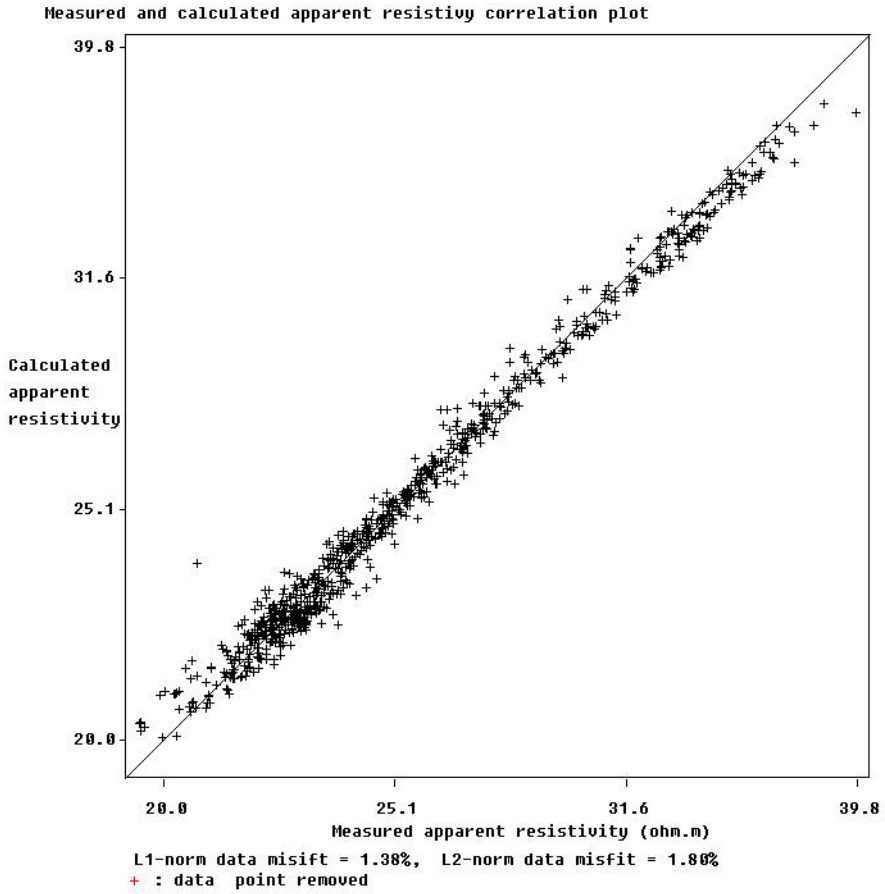


**Figure 3.6 A scatter plot showing the fitting between the measured and calculated resistivities**

## 3.3 Results

3.2.1 Synthetic Experiments

By applying COMSOL Multiphysics to the water flow and resistivity model shown in (Figure 3.1) for the 3D forward modeling numerical simulation, canal water flows in a higher velocity beside the canal where this Flow velocity is getting higher throughout the Basalt unit than it is in the Sand unit (Figure 3.7). This may be attributed to the fact that the fractured basalt has larger fractures or pores that result in lower negative pressure or tension between the water molecules and the surrounding grains. The distributions of electric potential differences obtained from these simulations were converted to resistance

given the current injected to the ground. The resistance values were used to determine the apparent resistivity distribution for the 4 endmembers; Sand, Silt, and Gravel unit and Basalt unit in both dry and wet conditions. The apparent resistivity distributions for them are shown in (Figures 3.8-3.9) where the maximum investigation depth was 23 m below the ground surface. The apparent resistivity values in the Sand, Silt, and Gravel unit before the irrigation season are ranging from (172-2852.5 Ohm.m) (Figure 3.8), but these values decrease to (149-2171 Ohm.m) in conjunction with water being present in the adjacent canal (Figure 3.9). This decline in the resistivity values is attributed to the canal seepage which is significantly observable when getting closer to the canal located at the NW. High resistivity values near ground surface are due to dry soil, and these values decrease with increasing depth while getting closer to the water table which is assumed to be at 25 m below ground surface. Compared to the Sand unit, the apparent resistivity values in the Basalt unit are ranging from (17-1132.6 Ohm.m) in the dry conditions (Figure 3.10), but these values dramatically decrease (16.5-662 Ohm.m) in the irrigation season (Figure 3.11) because of the canal seepage effect which is significantly high when getting closer to the canal located at the NW, and probably because of the fact that the fractured basalt has secondary porosity; more permeable than sand, silt and gravel unit which may have lower permeability because of the grain sorting. High resistivity values near the ground surface are due to dry basalt. These values decrease with increasing depth while getting closer to the water table which is assumed to be at 10 m below ground surface. The basalt dominated system is more complicated in terms of the apparent resistivity distribution and it requires more carefulness and cautions when dealing with it. This complexity is believed to be

attributed to the fractures, pores arrangement and the Basalt material itself which influence the electric current flow propagation.

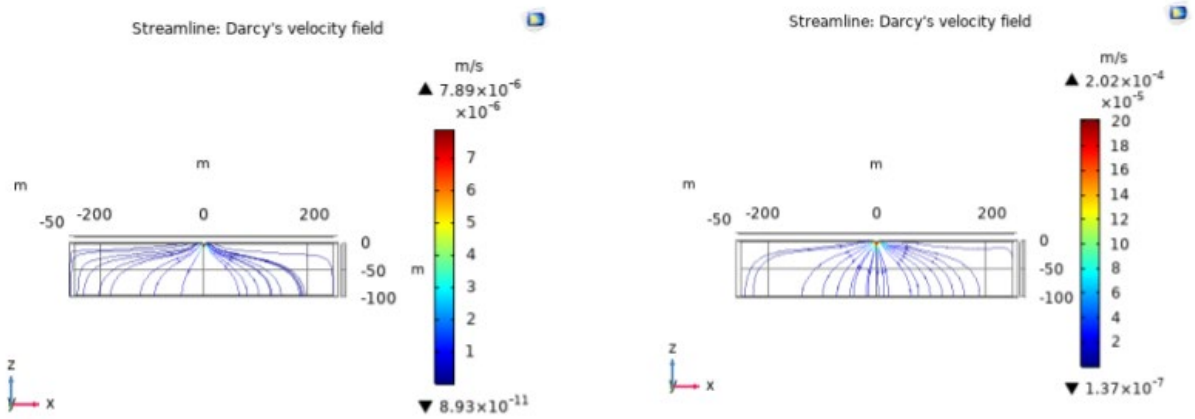


**I) Sand, Gravel & Silt unit** **II) Basalt unit**

**Figure 3.7 Flow Pattern and Velocity: I) Sand, Gravel & Silt unit, II) Basalt Unit**

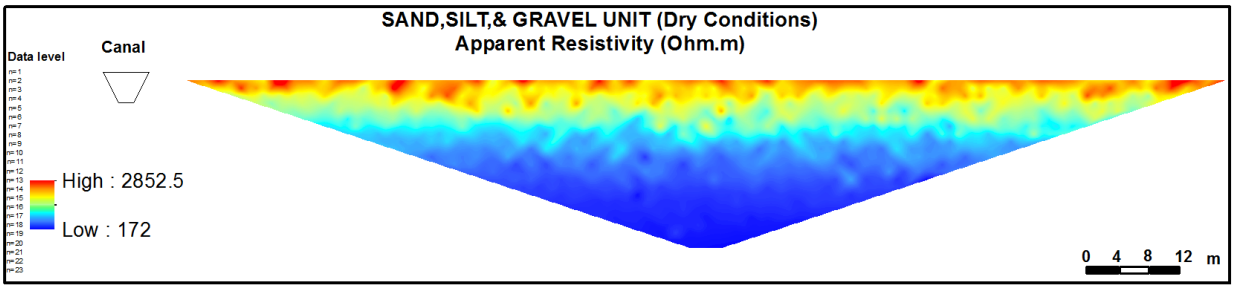


**Figure 3.8 Apparent Resistivity distribution in Sand, Silt, and Gravel unit in the dry conditions**

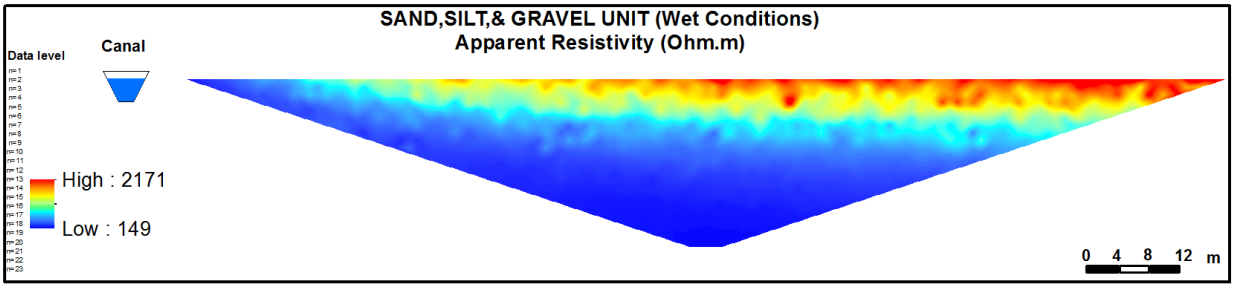


**Figure 3.9 Apparent Resistivity distribution in Sand, Silt, and Gravel unit in the wet conditions**

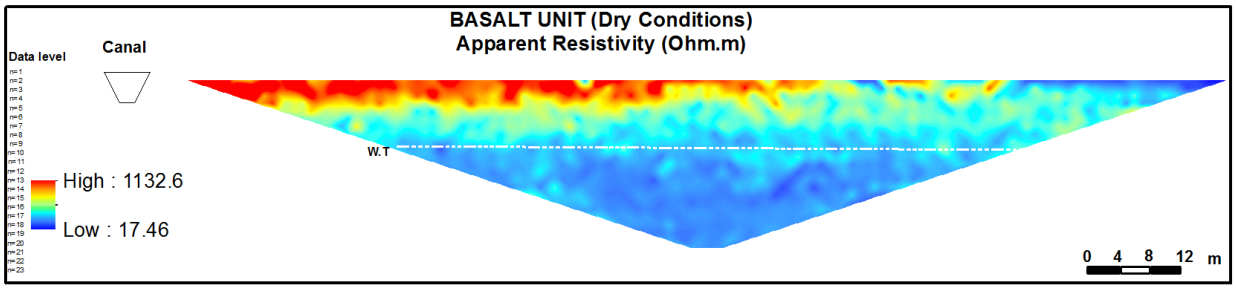


**Figure 3.10 Apparent Resistivity distribution in Basalt unit in the dry conditions**

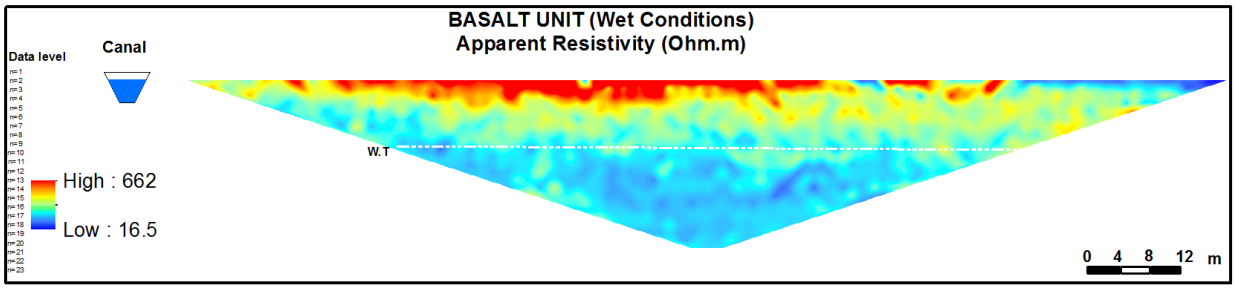


**Figure 3.11 Apparent Resistivity distribution in Basalt unit in the wet conditions**

3.2.2 DC Resistivity

Two-dimensional electrical tomography survey profiles were carried out perpendicular to the Phyllis Canal in Lions Park, Nampa (Basalt unit) (Photo 3.2) using Wenner Alpha over two months to monitor the temporal resistivity variation resulting from canal seepage. The apparent resistivity values range from 18 ohm-m to 37 ohm-m for both pseudo-sections (Figure 3.12). However, the apparent resistivity values decreased (except for the top layer) after 26 days of water being in the canal (Figure 3.12). The apparent resistivity distributions were inverted to get the closest geologic subsurface model to the actual measured values and to monitor the change in the saturation zone due to canal seepage over two months. Based on the inversion results (Figure 3.13), the uppermost lithologic layer is believed to be a dry surface layer of a wide range of resistivity values (~17-60 ohm-m) due to the lateral heterogeneity. However, most of this layer has higher resistivity values because of the fact of being dry. This layer extends up to approximately

7 m below ground surface. This layer did not show a change in the resistivity range it had after the irrigation season started, but there was a subtle change in the resistivity distribution on the corners of the after irrigation- 2D ERT profile; resistivity values were decreased and this may be because of the precipitation and irrigation with sprinklers that were dominating before the start of the experiment. This supports that the uppermost layer extending from (~ 30-120 m) in the X-direction is an impermeable layer. The second layer was interpreted as sand/gravelly sand of approximately 10 m depth extending from 7-17 m below ground surface. This middle layer has a low resistivity range upto 17 ohm-m. This layer had a perched saturated layer of lower resistivity value before the irrigation season. This perched layer was significantly enlarged laterally in the east direction with the irrigation season. The bottom layer with resistivity values ranging from (~40-65 ohm-m) was believed to be Loose lava. This lithologic unit's interpretation was calibrated with the ancillary well data (Figure 3.14) available in the vicinity of the 2D-ERT profile. The record in the well logs is provided by the drillers and the labels of its lithologic units are not always consistent with known lithologic units. We were interested in the canal seepage influence on the shallow GW aquifer more than the lithology distribution. The inversion results and the resistivity variation over approximately two months showed that the water from the Phyllis canal seeped and moved laterally to approximately 120 m to the east direction of the profile which supports that the canal seepage has a significant influence on the shallow GW aquifer recharge. The water table of this saturated sand/gravelly sand layer is believed to be at approximately 7 m below ground surface and the source of this aquifer is the canal seepage not fossil water. This can be proved by trace elements chemical analyses.

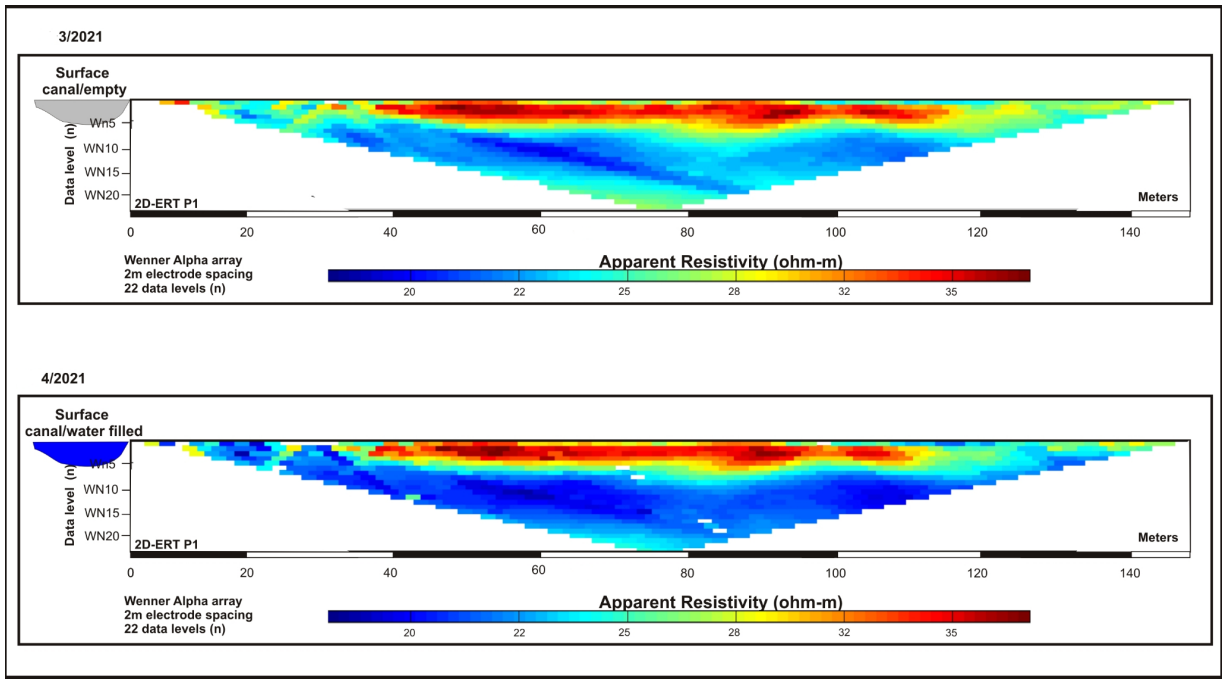


**Figure 3.12 Comparison of resistivity pseudosections obtained from Wenner Alpha array of 2D-ERT over March (i.e, dry canal) and April 2021 (i.e, water filled canal)**

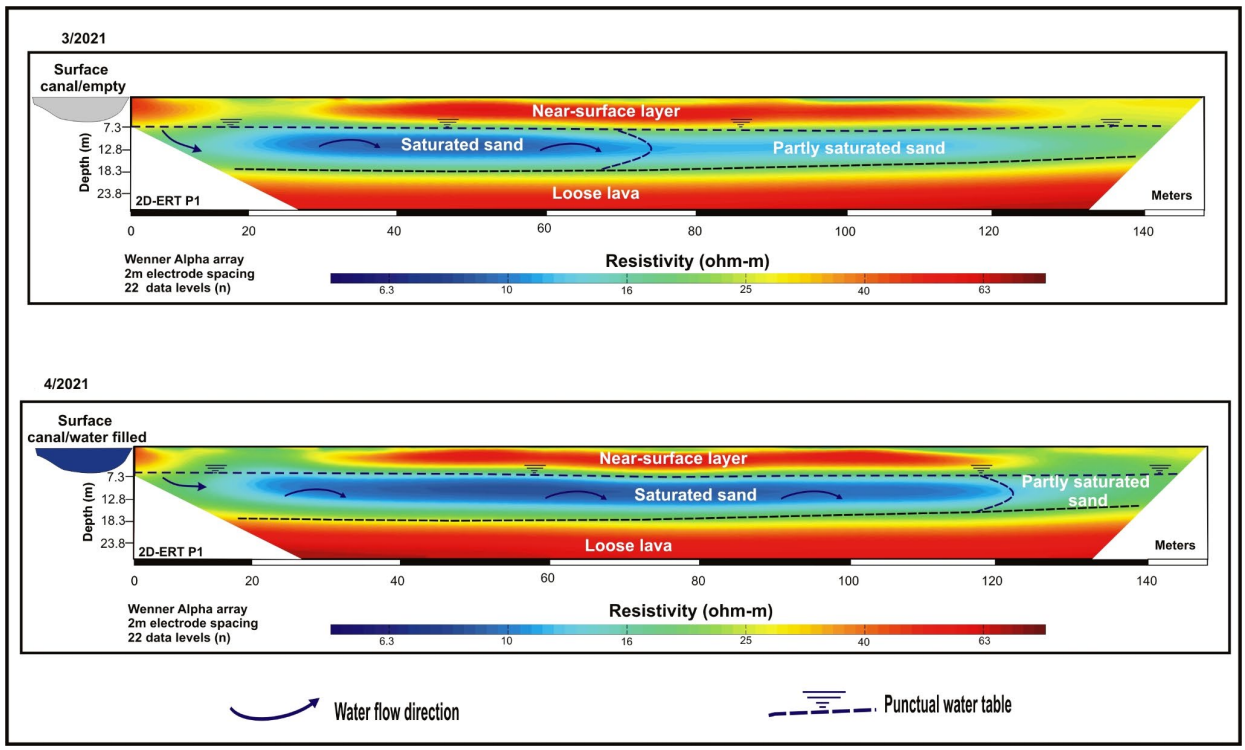


**Figure 3.13 Advanced time-lapse ERT inversion results over two months showing the resistivity variation as a result of the lateral water flow movement from the adjacent water-filled surface Phyllis canal**

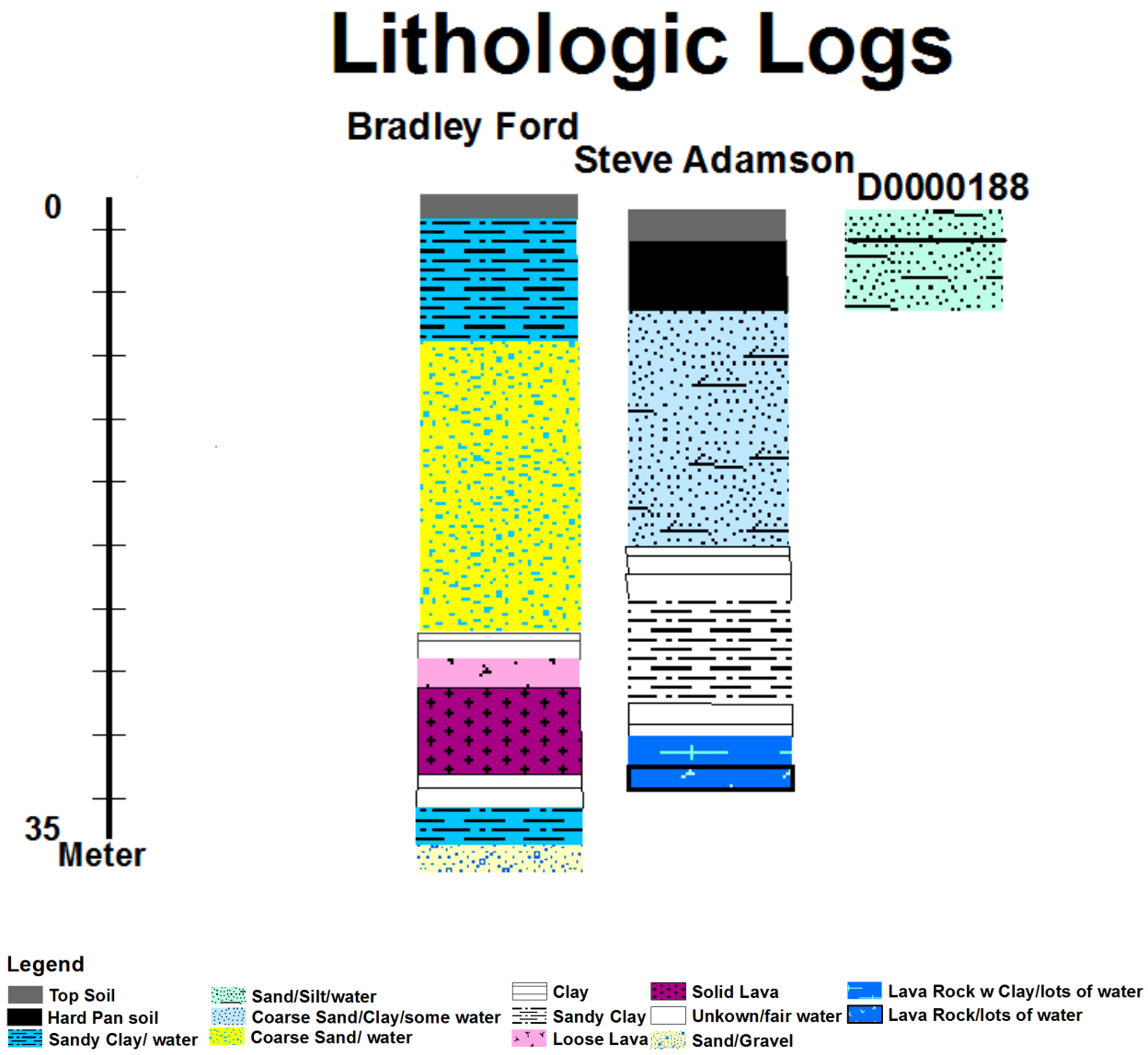


**Figure 3.14 Ancillary well data available in the vicinity of the 2D-ERT profile (their location is shown in (Figure 3.3)**

### 3.4 Discussion

Managing the existing water resources efficiently in the agricultural landscapes, water budget components (i.e; inflows and outflows) should be accurately quantified. Canal seepage is the key input in the TV's water budget and its estimation is crucial (Urban,

2004). In chapter 2, we estimated seepage via selected canal reaches of different properties using the gain/loss method where the total gain/loss across the TV was estimated using 3 scaling methods. However, there is uncertainty associated with these estimations especially in the Basalt unit and Sand, Silt, and Gravel unit. We believe that additional measurements are necessary to better constrain the canal seepage variability and uncertainty.

In this chapter, we started with a hydrogeophysical simulation using COMSOL Multiphysics in 2 lithologic units over 2 different conditions (i.e, dry vs. irrigation season). The four end members created by this simulation showed a substantial complexity associated with the Basalt unit during the irrigation season. We deployed Direct Current (DC) Resistivity measurements in one location in this unit over two months (i.e, March, and April 2021) to monitor the subsurface resistivity changes which are attributed to variation in the saturation and water content as a result of the canal subsurface seepage. The advanced time-lapse ERT inversion results over approximately two months showed that the saturated zone was laterally expanded as a result of the lateral water flow movement from the adjacent water-filled surface Phyllis Canal (Figure 3.13). The canal seepage has a significant influence on the shallow GW aquifer recharge. The inversion results of the 2D-ERT method can be useful for further investigation to get a quantitative seepage estimate across this Basalt. We made a rough calculation based on the change of the saturated layer geometry over time and some assumptions. Our key assumptions are: (1) the time-lapse 2D-ERT geophysical method provides a reasonable approximation of the additional saturated area due to canal seepage, (2) although we do not know the initial conditions in terms of what the soil moisture was when the adjacent canal was dry, we assume that the soil was completely dry (i.e; the initial soil moisture is zero) then it became

fully saturated after diverting water into the canal, (3) water table of the saturated sand/gravelly sand layer is believed to be at approximately 7 m below ground surface, (4) the width and depth of this saturated zone are approximately 52 and 11 m, respectively, (5) the length of the canal reach is assumed to be the average length of the two measured reaches in this Basalt unit (228.25 m of both Indian Creek and 15 Lateral), (6) the porosity of the sand/gravelly sand layer is assumed to be 0.4 (i.e, permeable sand/gravelly sand layer) based on the inversion results, (7) seepage time is 26 days (April, 1st to April, 26th), and (8) both of the canal sides are symmetric. Using these assumptions, we calculated a rough estimate of the seepage rate across this lithologic unit.:

Q_ERT = 52 m x 11 m x 228.25 m x 0.4 x 2 / (26 x 24 x 60 x 60 s) = 0.046 cms

Where Q_ERT is the seepage in cms using the ERT method.

The seepage estimate is approximately 1.954 × 10^-4 cms for this subsurface profile slice, while the seepage rate across a reach of this average length in this unit using the ERT method is approximately 0.05 cms. This rate is slightly different but comparable to 0.11, and 0.07 cms of Indian Creek and 15 Lateral, respectively. However, we anticipate significant uncertainty in this seepage estimation because we assume that the subsurface conditions across and along the canal are homogeneous and we do not know the initial soil moisture conditions. While this very simple calculation provides seemingly reasonable estimates, we strongly recommend doing additional measurements to constrain this uncertainty by deploying additional ERT profiles in the future at this site to capture the lateral heterogeneity along and across both the canal sides; 2 profiles across the canal on the same side as the 1st profile, and the other 3 profiles across the other side of the canal.

Additionally, we need information on the initial conditions of the soil moisture. Furthermore, examining trace elements for water samples collected from the adjacent wells to confirm the ERT inversion results which demonstrate that the source of the saturated sand/gravelly sand aquifer layer is the canal seepage not fossil water. Canal seepage impacts the local aquifers wherever there is an extensive canal system such as the TV and the Western United States, and to better understand how big that impact is, we need a high resolution geospatial database for layers of canals, drains, and ditches. Cooley et al. (2017) concluded that Planet CubeSat imagery provides a powerful tool for monitoring the dynamic surface water bodies, although there are some limitations associated to this imagery such as the geolocation inaccuracies, lack of an automated cloud mask, and inconsistent radiometric calibration across multiple platforms which should be addressed. High resolution remote sensing images such as Planet CubeSat imagery– coupled with image classification machine learning methods – might be useful in automatically generating estimates of canal widths.

## References

Akinola, B. S., Awoyemi, M. O., Matthew, O. J., & Adebayo, A. S. (2018). Geophysical and hydro-chemical investigation of contamination plume in a basement complex formation around Sunmoye dumpsite in Ikire, Southwestern Nigeria. *Modeling Earth Systems and Environment*, *4*(2), 753-764.

Audenrieth, I., Martin, R., Yogeshwar, P., & Willig, D. (2020). Analysis of measurement errors from electrical resistivity imaging investigation of First World War mining tunnels in La Boisselle, France. *Near Surface Geophysics*, *18*(5), 561-573.

Attwa, M., El Bastawesy, M., Ragab, D., Othman, A., Assaggaf, H. M., & Abotalib, A. Z. (2021). Toward an Integrated and Sustainable Water Resources Management in Structurally-Controlled Watersheds in Desert Environments Using Geophysical and Remote Sensing Methods. *Sustainability*, *13*(7), 4004.

Attwa, M., & Günther, T. (2012). Application of spectral induced polarization (SIP) imaging for characterizing the near-surface geology: an environmental case study at Schillerslage, Germany. *Australian Journal of Basic and Applied Sciences*, *6*(9), 693-701.

Freeze, R. A., & Cherry, A. JA 1979. Groundwater. *Prentice Hall, Inc, Upper Saddle River, NJ*, *7458*, 213.

Attwa, M., & Zamzam, S. (2020). An integrated approach of GIS and geoelectrical techniques for wastewater leakage investigations: Active constraint balancing and genetic algorithms application. *Journal of Applied Geophysics*, *175*, 103992.

Binley, A., & Kemna, A. (2005). DC resistivity and induced polarization methods. In *Hydrogeophysics* (pp. 129-156). Springer, Dordrecht.

Butler, S. L., & Sinha, G. (2012). Forward modeling of applied geophysics methods using Comsol and comparison with analytical and laboratory analog models. *Computers & Geosciences*, *42*, 168-176.

Clément, R., Descloitres, M., Günther, T., Oxarango, L., Morra, C., Laurent, J. P., & Gourc, J. P. (2010). Improvement of electrical resistivity tomography for leachate injection monitoring. *Waste management*, *30*(3), 452-464.

COMSOL Multiphysics User's Guide (2017) Version 5.3. COMSOLAB, Stockholm.

Cooley, S. W., Smith, L. C., Stepan, L., & Mascaro, J. (2017). Tracking dynamic northern surface water changes with high-frequency planet CubeSat imagery. *Remote Sensing*, *9*(12), 1306.

Dey, A., & Morrison, H. F. (1979a). Resistivity modelling for arbitrarily shaped two-dimensional structures. *Geophysical Prospecting*, *27*(1), 106-136.

Dey, A., & Morrison, H. F. (1979b). Resistivity modeling for arbitrarily shaped three-dimensional structures. *Geophysics*, *44*(4), 753-780.

El-Saadawy, O., Gaber, A., Othman, A., Abotalib, A. Z., El Bastawesy, M., & Attwa, M. (2020). Modeling Flash Floods and Induced Recharge into Alluvial Aquifers Using Multi-Temporal Remote Sensing and Electrical Resistivity Imaging. *Sustainability*, *12*(23), 10204.

Gao, J., Smirnov, M., Smirnova, M., & Egbert, G. (2020). 3-D DC resistivity forward modeling using the multi-resolution grid. Pure Appl Geophys 177:2803–2819.

Gautam, P. K., & Biswas, A. (2016). 2D Geo-electrical imaging for shallow depth investigation in Doon Valley Sub-Himalaya, Uttarakhand, India. *Modeling Earth Systems and Environment*, *2*(4), 1-9.

Günther, T. (2004). Inversion methods and resolution analysis for the 2D/3D reconstruction of resistivity structures from DC measurements. Ph.D. thesis, Technische Univ., Freiberg, Germany.

Günther, T. (2007). DC2DInvRes-Direct current 2D inversion and resolution.

Hübner, R., Günther, T., Heller, K., Noell, U., & Kleber, A. (2017). Impacts of a capillary barrier on infiltration and subsurface stormflow in layered slope deposits monitored with 3-D ERT and hydrometric measurements. *Hydrology and Earth System Sciences*, *21*(10), 5181-5199.

Loke, M. H. (2004). Tutorial: 2-D and 3-D electrical imaging surveys.

Moreira, C. A., Casagrande, M. F. S., & Borssatto, K. (2020). Analysis of the potential application of geophysical survey (induced polarization and DC resistivity) to a long-term mine planning in a sulfide deposit. *Arabian Journal of Geosciences*, *13*(20), 1-12.

Multiphysics, C. O. M. S. O. L. (2018). Subsurface Flow Module User's Guide. *Version: COMSOL*, *5*.

Oladunjoye, M. A., Salami, A. J., Aizebeokhai, A.P., Sanuade, O.A., & Kaka, S.I. (2017) Preliminary geotechnical characterization of a site in southwest Nigeria using integrated electrical and seismic methods. J Geol Soc India 89:209–215

Olaojo, A. A., Oladunjoye, M. A., Sanuade, O. A. (2018). Geoelectrical assessment of polluted zone by sewage efuent in University of Ibadan campus southwestern Nigeria. Environ Monit Assess 190:24

Olaseeni, O. G., Sanuade, O. A., Adebayo, S. S., & Oladapo, M. I. (2018). Integrated geoelectric and hydrochemical assessment of Ilokun dumpsite, Ado Ekiti, in southwestern Nigeria. Kuwait. J Sci 45(4):82–92

Oyeyemi, K. D., Aizebeokhai, A. P., Adagunodo, T. A., Olofinnade, O. M., Sanuade, O. A., & Olaojo, A. A. (2017). Subsoil characterization using geoelectrical and geotechnical investigations: implications for foundation studies. Int J Civ Eng Technol 8(10):302–314

Oyeyemi, K. D., Aizebeokhai, A. P., Olofnnade, O. M., & Sanuade, O. A. (2018a). Geoelectrical investigations for groundwater exploration in crystalline basement terrain, SW Nigeria: implications for groundwater resources sustainability. Int J Civ Eng Technol 9(6):765–772

Oyeyemi, K.D., Aizebeokhai, A. P., Ndambuki, J. M., Sanuade, O. A., Olofnnade, O. M., Adagunodo, T. A., Olaojo, A. A., & Adeyemi, G. A. (2018b). Estimation of aquifer hydraulic parameters from surfcial geophysical methods: a case study of Ota, Southwestern Nigeria. IOP Conf Ser Earth Environ Sci 173:1–10.

Oyeyemi, K. D., Olofnnade, O. M., Aizebeokhai, A. P., Sanuade, O. A., Oladunjoye, M. A., Ede, A. N., Adagunodo, T. A., & Ayara, W. A. (2020). Geoengineering site characterization for foundation integrity assessment. Cogent Eng 7:1–16.

Rosales, R. M., Martınez-Pagan, P., Faz, A., & Moreno-Cornejo, J. (2012). Environmental monitoring using electrical resistivity tomography (ERT) in the subsoil of three former petrol stations in SE of Spain. Water Air Soil Pollut 223(7):3757–3773. https ://doi.org/10.1007/s1127 0-012-1146-0.

Sanuade, O. A., Amosun, J. O., Fagbemigun, T. S., Oyebamiji, A. R., & Oyeyemi, K. D. (2021). Direct current electrical resistivity forward modeling using comsol multiphysics. *Modeling Earth Systems and Environment*, *7*(1), 117-123.

Silvester, P. P., & Ferrari, R. L. ( 1990). Finite elements for electrical engineers (2nd. ed.). Cambridge University Press.

Song, T. Liu, Y. Wang, Y. (2017). Finite element method for modeling 3D resistivity sounding on anisotropic geoelectric media. Math Probl Eng 2017:1–13. https ://doi.org/10.1155/2017/80276 16.

Telford, W. M., Geldart, L. P. & Sheriff, R.E. (1990). Applied Geophysics (second edition). Cambridge University Press.

Udosen, N. I. & George, N. J. (2018). A finite integration forward solver and a domain search reconstruction solver for electrical resistivity tomography (ERT). Model Earth Syst Environ 4:1–12.

Wang, X., Yue, H., Liu, G. & Zhao, Z. (2011). The application of COMSOL Multiphysics in direct current method forward modeling. Procedia Earth Planet Sci 3:266–272.

# CONCLUSION

Monitoring SW-GW interactions in arid environments is essential for effectively managing the existing water resources. Quantifying how much surface water is being exchanged with the shallow GW aquifer is crucial for water conservation in the agricultural landscapes. Previous water budgets estimated this term based on assumptions that did not incorporate canal variability and flow measurement uncertainty. To address this, we deployed seepage measurements on 6 canal reaches of different sizes and underlying lithology in the TV using gain/loss method. The discrete measurements were scaled using 3 alternative ways for estimating the total seepage across the TV while taking into consideration the measurement uncertainty. Our findings show high seepage variability across the canals which is valuable for choosing the best management strategies that should be implemented in this heavily managed system. For instance, canals of significant seepage rate such as the Fivemile Feeder may be a promising recharge location for replenishing the shallow GW aquifer when there is a local decline in the water table. Considering seepage variability, and measurement uncertainty in quantifying seepage magnitude showed that the previous water budgets underestimated the TV canal seepage. Moreover, this seepage study showed how valuable inclusion of small canals is in seepage estimation; they contribute approximately 63% of the total G/L on average across the TV. Uncertainty analyses showed that flow measurements in the Basalt unit (i.e; Indian Creek) and Sand, Silt, and Gravel unit (i.e, 5.17 Lateral) are significantly uncertain.

To examine how hydrogeophysical simulation may be useful for monitoring SW-GW interactions in managed water resource systems, we used COMSOL Multiphysics to get the subsurface resistivity distribution in two different conditions and lithology. This forward modeling showed that the Basalt unit is a complex system during the irrigation season. To address uncertainty of seepage estimation using gain/loss method, we used the DC resistivity method to test how efficient the integration between the DC and gain/loss methods in water resources management is. We deployed these measurements in one location in the Basalt unit before and after the irrigation season started to monitor the change of the subsurface saturation upon the water diversion in the irrigation canals. The ERT inversion shows that the canal water moved laterally a distance of 50 m and this surface water is affecting the shallow GW aquifer; it is believed to be the source of the saturated sand/gravelly sand aquifer layer. Rough seepage rate estimation was done using the ERT results where the seepage rate showed a good agreement with its estimation using gain/loss in the Basalt unit. We recommend doing additional measurements at the same site to capture the subsurface heterogeneity and constrain the uncertainty. Moreover, deploying DC measurements should be implemented in the Sand, Silt, and Gravel unit especially in the vicinity of 5.17 Lateral to capture the subsurface conditions and examine whether the adjacent Phyllis canal affects the G/L uncertainty in this reach or not. Further measurements should be done across the 6 measured reaches to decrease the G/L uncertainty estimation across the whole TV. This research evaluates how the integration of different methods may provide additional insight into GW - SW exchange which will help evaluate alternative management options for achieving sustainable management of existing water resources.

# APPENDIX A1

## Temporal Variability of Upstream and Downstream Discharge Distributions across the Measured Canal Reaches

The upstream and downstream discharge distributions were created for each reach weekly to capture the temporal variability within each reach per time if present. This following 6*6 (Figure A1.1) demonstrates that the most uncertain reaches are Indian Creek, and 5.17 Lateral, while it is obvious that Fivemile feeder is consistently losing each week. So, the confidence level of estimating whether Indian Creek, or 5.17 Lateral are losing or gaining and how much water is being exchanged through them and the shallow GW aquifer.

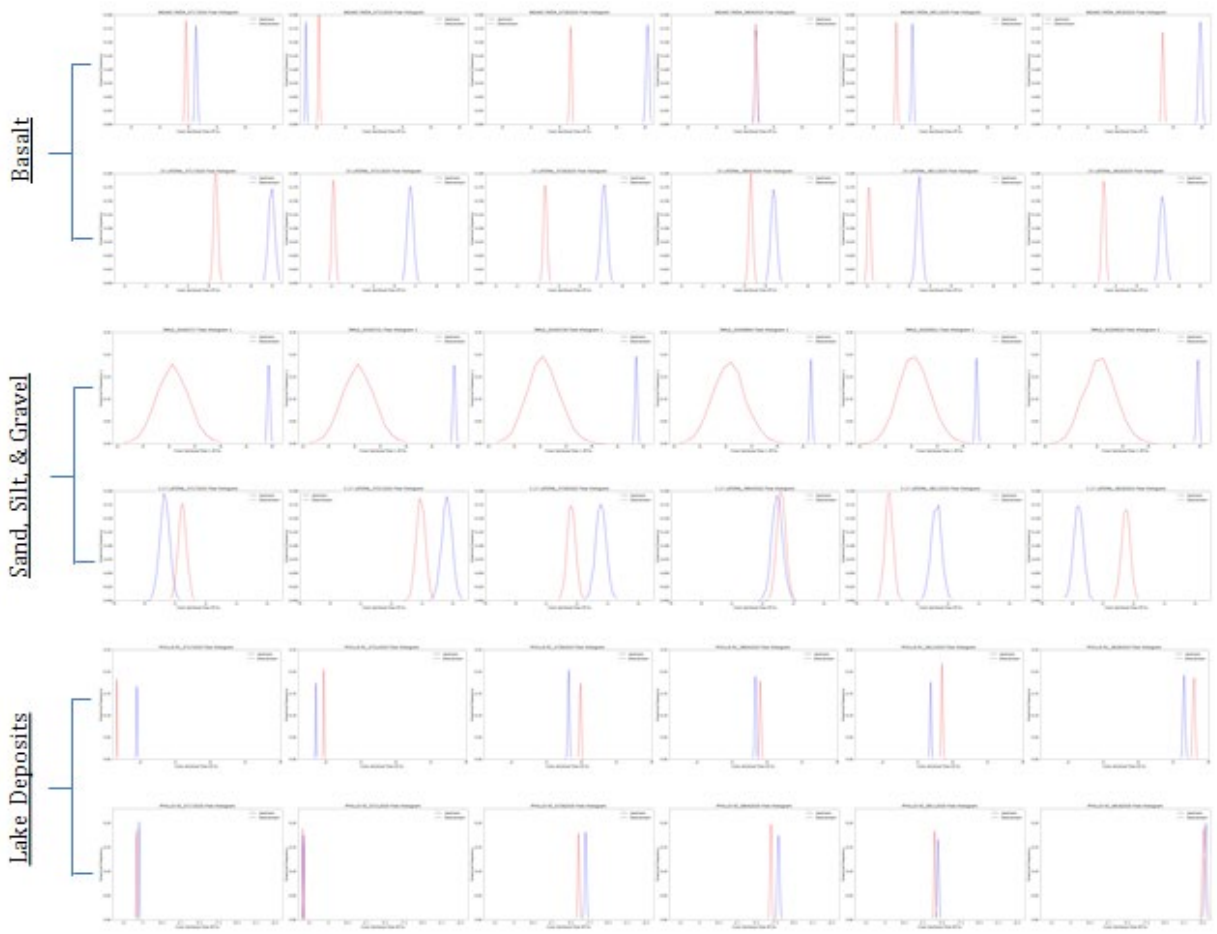


**Figure A1.1 Upstream and downstream discharge distribution variability with time within each measured reach and between all of them**

# APPENDIX A2

## Uncertainty Analyses at Fivemile Feeder

Streamflow at Fivemile downstream location was unmeasurable due to the channel bed condition, so a weighting curve equation provided by the Pioneer district was used to get the discharge. Since the discharge at this downstream section was calculated using an equation which has a depth variable (D) and weighting curve parameters (A, and B), its discharge uncertainty was quantified using three alternative approaches. The first approach was done by perturbing a depth error by adding a normal random number of different standard deviations (i.e; 0.015, 0.003 m) while keeping the other parameters constant. The second method was to perturb the parameters by adding different percentage errors to parameter A (i.e; 5, 10, 15 %) and exponent B (i.e; 1, 2, 5%) while keeping the depth variable unchanged. The third approach involved introducing reasonable errors into both depth and parameters. For uncertainty analysis at this site, the depth error was AWG, while the parameters' errors were multiplicative ones. Monte Carlo simulation (MCS) of 5000 times were applied to estimate uncertainty in depth and the weighting curve parameters.

For Fivemile Feeder, the discharge distribution of the upstream was compared to those 3 distributions of the downstream discharge which were created using the 3 different approaches. Statistics of the downstream discharges using 3 approaches of error propagation were compared to detect the variable of the major contribution in the discharge uncertainty. For instance, table (A2.1) shows the means and standard deviations of approach A, B, and C assuming 10% error in A, 1% error in B, and 0.18 m error in depth. Figure (2.3) showing G/L histograms for each sampling date at Fivemile Feeder was presented in Chapter 2 in the methods section to show G/L variability with time. Based on the uncertainty analysis shown in table (A2.1), We used approach A for getting the

downstream distribution used for estimating G/L at this site because it captured most of the uncertainty as the depth error was the key factor affecting the discharge uncertainty more than the errors in the other parameters.

**Table A2.1 Statistics of Fivemile Feeder Downstream Discharges using 3 approaches (Example: 10% error in A, 1% error in B, 0.18 m error in depth)**

| Fivemile Feeder (Downstream Discharge) | | | | |
|---|---|---|---|---|
| Date | m^3/s | Approach A | Approach B | Approach C |
| 07/17 | Mean | 0.869 | 0.867 | 0.870 |
| | Std. | 0.088 | 0.049 | 0.10 |
| 07/21 | Mean | 0.868 | 0.866 | 0.867 |
| | Std. | 0.087 | 0.0498 | 0.099 |
| 07/28 | Mean | 0.869 | 0.866 | 0.868 |
| | Std. | 0.088 | 0.05 | 0.10 |
| 08/04 | Mean | 0.869 | 0.867 | 0.869 |
| | Std. | 0.086 | 0.05 | 0.10 |
| 08/11 | Mean | 0.87 | 0.867 | 0.870 |
| | Std. | 0.087 | 0.049 | 0.10 |
| 08/18 | Mean | 0.868 | 0.867 | 0.868 |
| | Std. | 0.088 | 0.05 | 0.10 |

# APPENDIX A3

**Grouping Lithologic Units for Scaling Measurements to the whole TV**

We measured flow discharge in canals located in the dominant 3 lithologic units in Pioneer district, this creates challenges for scaling the measurements for the whole TV where there are 9 lithologic units. To address this, we grouped similar lithologic units together and added them to the most similar unit of the major 3 lithologic units in the TV (table A3.1) to obtain the total G/L for the entire valley. G/L using the 3 alternative methods of scaling across the 3 lithologic units were compared to those across the whole TV (Table A3.2) and (Figure A3.1). This figure shows how significant the G/L of these major lithologic units is to the total TV's G/L.

**Table A3.1 Grouping similar lithologic units for scaling process**

| Group Name | Source Code |
|---|---|
| Sediments and Sedimentary rocks | Sediments and Sedimentary rocks<br>Landslide deposits<br>Alluvials<br>Alluvial fans |
| Basement | Basalt<br>Granodiorite<br>Granite |
| Lake Deposits | Lake deposits<br>Fluvial deposits |

**Table A3.2 Comparison of gain/Loss quantified using the 3 approaches of scaling across the 3 major lithologic units and across the whole TV**

| | Study or Method | G/L (acre ft/yr) | G/L (acre ft/yr) *-10^3 |
|---|---|---|---|
| The whole TV | Method A` | -3,233,316 | 3,233 |
| | Method B` "scaled by lithologic unit" | -11,753,372 | 11,753 |
| | Method C` "scaled by lithology and canal size" | -11,134,458 | 11,134 |
| For 3 Lithologic units | Method A | -2,200,916 | 2,201 |
| | Method B "scaled by lithologic unit" | -7,187,070 | 7,187 |
| | Method C "scaled by lithology and canal size" | -6,205,547 | 6,206 |

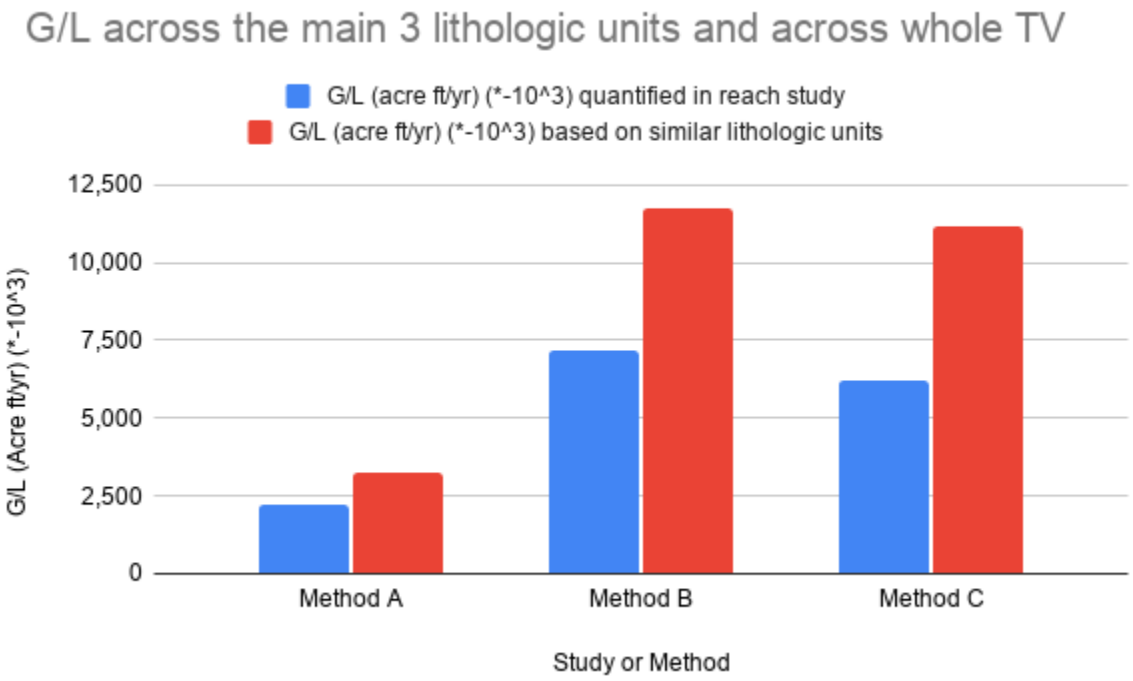


**Figure A3.1 A bar chart shows G/L across the main 3 lithologic units and across the whole TV**